

Atom focusing by far-detuned and resonant standing wave fields: Thin lens regime.

J. L. Cohen[†], B. Dubetsky^{*}, and P. R. Berman^{*}

[†]*Applied Physics Program, Department of Physics, University of Michigan, Ann Arbor, MI 48109-1120*

^{*}*Department of Physics, University of Michigan, Ann Arbor, MI 48109-1120*

(April 30, 2019)

The focusing of two-level atoms in a beam or trap after interacting with both far-detuned and resonant standing wave fields in the thin lens and paraxial approximations is considered theoretically. The thin lens approximation is discussed quantitatively from a quantum perspective. Exact quantum expressions for the Fourier components of the density (that include all spherical aberration) are used to study the focusing numerically. The following lens parameters and density profiles are calculated as functions of the pulsed field area θ : the position of the focal plane, peak atomic density, atomic density pattern at the focus, focal spot size, depth of focus, and background density. The lens parameters are compared to asymptotic, analytical results derived from a scalar diffraction theory for which spherical aberration is small but non-negligible ($\theta \gg 1$). Within the diffraction theory analytical expressions show that the focused atoms in the far detuned case have an approximately constant background density $0.5(1 - 0.635\theta^{-1/2})$ while the peak density behaves as $3.83\theta^{1/2}$, the focal distance or time as $\theta^{-1}(1 + 1.27\theta^{-1/2})$, the focal spot size as $0.744\theta^{-3/4}$, and the depth of focus as $1.91\theta^{-3/2}$. Focusing by the resonant standing wave field leads to similar results. However, resonant focusing is also accompanied by a new effect, a Rabi-like oscillation of the atom density. For the far-detuned lens, chromatic aberration caused by the longitudinal velocity distribution in an atom beam is studied quantitatively with the exact Fourier results. Similarly, the degradation of the focus that results from angular divergence in beams or thermal velocity distributions in traps is studied quantitatively with the exact Fourier method and understood analytically using the asymptotic results. Overall, we show that strong thin lens focusing is possible with modest laser powers and with atomic beam characteristics that are currently achievable in the laboratory.

03.75.Be, 32.80.Lg

I. INTRODUCTION

Evolving from the initial experiments [1,2], the study of atom focusing using standing wave (SW) light fields has developed into a broad area of research in atom optics. A standing wave field acts as a lens as a result of a spatially-dependent light shift, focusing atoms into a periodic set of lines or dots having widths of the order of tens of nanometers and distanced from one another by $\lambda/2$, where λ is the wave length of the light. Focusing by thick lenses and atomic deposition on a substrate have been observed for beams of Na [1,3–7], metastable He [2], and Cr [8–10]. The latest achievements in this area are summarized in a recent review article [11]. Perhaps even more significantly, lithographic techniques have been developed to create nanosurfaces in semiconductors and metals using metastable atoms as a pattern template for selective etching [12]. Similarly, cold, trapped atoms can be subjected to SW light pulses [13,14], creating a periodic wave packet which will focus along the field propagation direction at specific times following the atom-field interaction.

Previous experiments with atomic beams have been carried out in a thick lens regime for which the atoms focus within the laser beam. Since the substrate surface is typically placed near the plane of peak intensity of the

thick SW lens and mechanically fixed to the retroreflecting mirror, in some sense these experiments are easier to set up when compared to thin lens experiments. The classical and quantum motion through a thick lens have been numerically simulated and compared to experimental data in Refs. [7,15–18]. The classical motion and lens parameters after thick and thin lenses have also been studied in detail within a ray optics formalism [19]. For that work the lens characteristics and aberrations beyond the parabolic lens approximation were simulated numerically as were the effects of different atomic velocity distributions. However, a comprehensive theoretical study of the thin SW lens from a quantum perspective that details corrections to the lens parameters as a result of spherical aberration, chromatic aberration, and angular beam divergence has not appeared previously.

In this article we stress the flexibility and validity of a thin lens approach, where the atoms are detected or used for lithography after the interaction with the field. We derive exact and computationally expedient results for atomic matter waves by quantizing the center-of-mass motion from the outset, a process that naturally accounts for spherical aberration. Our hope is to stimulate interest in thin lens experiments by introducing a straightforward, yet rigorous theoretical framework for the problem and by deriving analytical results for lens parameters to

facilitate lithographic and atom optical configurations. The thin SW lens creates high contrast periodic structures in free flight and opens up numerous possibilities for Fourier atom optics to image and manipulate modulated matter waves. This approach is highly desirable, especially when coupled with advances in Bose-Einstein condensate (BEC) atom laser sources [14,20] with large fluxes and narrow velocity distributions. To our knowledge similar studies have been carried out only numerically using a Fresnel diffraction theory in the coordinate representation for a "doughnut"-mode optical field [21], standing wave field [22], and conical lens [23].

Rather than using the diffraction theory simply for numerical propagation of the matter waves, we extend its usefulness by deriving approximate analytical expressions for the SW field lens parameters. The Fresnel-Kirchhoff integral, incorporating the lowest-order spherical aberration, gives a relatively simple form for the atomic wave function near the focal plane and SW intensity extrema. Asymptotically for large atom-field pulse areas, this integral leads to a universal atomic density profile, revealing the behavior of the focal distance, peak atomic density, focal spot size [half-width at half-maximum (HWHM) of the atom density at the focus], depth of focus, and background density as a function of the pulse area. The analytical asymptotic results can then be compared to either numerical asymptotic approximations of the Fresnel integral or to the exact atomic distributions and lens parameters, most easily evaluated using a Fourier approach.

The time evolution of a free particle's wave function, when subject to a spatially periodic initial condition such as that imposed on an atom beam after passing through a SW field or microfabricated grating [13,24,25], can be expressed in terms of a Fourier expansion in the (plane wave) spatial harmonics of the modulation period. As such, the results we derive are closely related to the canon of research on periodic light optics [26]. In the thin lens approximation the Fourier components can be calculated exactly for the wave function and density and then superposed to evaluate the atomic spatial distribution: for this approach the calculations effectively take place in a momentum representation, whereas a numerical integration over the free particle propagator gives results in a coordinate representation. The expressions for the density's Fourier components that we use below were obtained recently for far-detuned [27] and resonant [28] SW fields. To our knowledge this exact solution has not been used previously to examine periodic focusing parameters, nor to compare with approximate solutions of focused waves. However, the Fourier components and the degradation of this type of focusing have been proposed recently as a way to study the onset of many-body effects in condensates [29].

The Fourier approach has several advantages. First, the time dependence of the Fourier coefficients directly reveals the quantum nature of the periodic atomic density as it varies explicitly with the atomic recoil energy of integer pairs of photons. Second, summation of the

Fourier series leads to fast convergence of the Fresnel solutions to arbitrary accuracy for all times when compared to the numerical integration of the full Fresnel-Kirchhoff integral. With this Fourier method for example, we can reproduce the main Fresnel diffraction results of Ref. [22] without having to integrate the partial differential equation or equivalent integral equation on a lattice. Furthermore, the Fourier method can be employed for the general case of typical atomic beam experiments, where the incident beam or trapped atoms are most accurately specified by a density matrix in momentum space, such as a thermal velocity distribution. The implications are that the spatial extent of the atomic distribution is much larger than the wavelength of the standing wave and the wave function is not transform limited (except perhaps for the case of a condensate), so that the focal densities are conveniently found as a function of this initial density matrix. As a direct result, while the failure to account for finite beam size effects with the Fourier series limits our calculations to the near-field and Fresnel diffraction regimes, it is relatively unimportant for atom focusing immediately following the SW pulse. We can then calculate the effects of chromatic aberration and angular beam divergence by averaging the exact Fourier solution over any longitudinal and transverse atomic velocity distributions.

In addition to lithographic detection schemes, one can detect atomic distributions modulated by SW fields by backscattering a pulsed traveling wave probe off of the density either (a) at a certain distance from the grating for the beam case or (b) after a certain time for the atoms released from a trap. The scattered signal is sensitive to the lowest-order Fourier component [30] of the modulated density. Previously, the backscattered signal from a cold vapor subjected to strong SW pulses was observed in Rb in a ground state echo experiment [13]. The excellent agreement between the Fourier theory and experiment that was achieved in that case insures that our theoretical approach can be applied to the atom focusing problem as well.

A new regime of atom focusing arises if the SW field is resonant with the transition between a ground and excited state and the time of interaction is less than the excited state lifetime. After propagating from the SW field for a time just long enough for the excited state to decay, the atom spatial distribution consists of two parts [28]: the stimulated density, caused by direct amplitude modulation of the ground state wave function by the field, and the spontaneous density, produced by excitation to and decay from the excited state. As a result of the periodic Talbot revival, or self-imaging [26,31,33,34], of the atomic spatial distribution, free evolution of the stimulated part leads to atom focusing not only at the focal distance L_f , but also at the distances $jL_T/2 \pm L_f$, where j is a positive integer, $L_T = \lambda^2/2\lambda_{dB}$ is a Talbot length, and λ_{dB} is the atom de Broglie wavelength. In contrast to the stimulated part, the spontaneous modulation decays at a distance on the order of L_T as a result of

the Doppler shift associated with spontaneous emission. At a sufficiently large distance, the modulated spontaneous part disappears, and one can observe and analyze atom focusing by a resonant SW field. This analysis then reveals a new effect, a Rabi-like oscillation of the focal parameters with the atom-field interaction strength that arises from an interference between different components of the matter wave.

This article is arranged as follows. In Section II we consider the focusing by a far-detuned field acting as a phase grating. Focusing by a resonant field acting as an amplitude grating is studied in Section III. Section IV is devoted to the influence of chromatic aberration (longitudinal velocity distributions) and angular beam divergence (transverse velocity distributions). The quantitative results and illustrative examples are discussed in Section V.

II. FAR-DETUNED STANDING WAVE LENS

Atom optical experiments can operate in the spatial or time domain. For example, in the time domain a vapor of cold atoms interacts with one or more radiation pulses forming spatial gratings in the x direction. Correspondingly, in the spatial domain an atom beam traverses one or more optical elements or interaction regions. For a monovelocity beam propagating along the z axis with longitudinal velocity U and with the optical elements aligned in the x direction, the spatial domain configurations can be analyzed in the time domain if calculations are performed in the atomic rest frame moving with velocity U . In this frame the optical elements appear as interaction pulses. As a result, our calculations are restricted to the time domain without loss of generality (and are adapted to account for a longitudinal velocity distribution in Section IV). We consider the focusing effects of a single pulse.

The atom optical elements couple to the center-of-mass degrees of freedom of an atom with mass M and de Broglie wavelength $\lambda_{dB} = 2\pi\hbar/(MU)$. When the SW laser field,

$$E(x, t) = Ee^{-i\Omega t}g(t)\cos(kx) + c.c., \quad (1)$$

drives the atomic transition between the ground state $|g\rangle$ and the excited state $|e\rangle$, the Schrödinger equation, $i\hbar\partial\Psi/\partial t = H\Psi$, governs the motion. The Hamiltonian in the rotating-wave approximation is

$$H = \frac{p_x^2}{2M} + \hbar\omega|e\rangle\langle e| + 2\hbar\chi g(t)\cos(kx)(e^{-i\Omega t}\sigma_+ + e^{i\Omega t}\sigma_-), \quad (2)$$

where

$$\Psi = \begin{pmatrix} \psi_e(x, t) \\ \psi(x, t) \end{pmatrix} \quad (3)$$

is the two-state wave function for the ground ($\psi(x)$) and excited ($\psi_e(x)$) states, p_x is the center-of-mass momentum operator, ω is the atomic transition frequency, $\Omega, k = q/2 = 2\pi/\lambda$, and $g(t)$ are the frequency, propagation wave vector, and pulse envelope function (centered at $t = 0$, having peak value of unity and duration on the order of τ), respectively, of the field, $\sigma_+(\sigma_-)$ is the atomic raising (lowering) operator associated with the transition $|g\rangle \rightarrow |e\rangle$ ($|e\rangle \rightarrow |g\rangle$), and $\chi = -\mu E/2\hbar$ is a Rabi frequency for the $|g\rangle \rightarrow |e\rangle$ transition with dipole matrix element μ . We have assumed for simplicity that the Rabi frequency χ is real.

In the spatial domain this Hamiltonian is written in the atomic rest frame for the slowly-varying wave function Ψ in the paraxial optics limit,

$$MU \gg \langle p_x \rangle, \sqrt{\langle p_x^2 \rangle - \langle p_x \rangle^2}; \quad (4)$$

for $t > 0$ the distance from the interaction region in the lab frame is $L = Ut$. In the time domain a paraxial approximation is unnecessary, and Ψ is simply the wave function. Experimentally [6], for focusing it has proven advantageous to optically pump the atoms into an initial ground state with magnetic quantum number $m_j = \pm j$ and use circularly polarized fields to avoid multiple Rabi frequencies in the state dynamics, justifying our two-level approximation.

Pure phase modulation of the atomic ground state during the interaction occurs in the far detuned case

$$\Delta \gg \max(\Gamma, \tau^{-1}), \quad (5)$$

where $\Delta = \Omega - \omega$ is the atom-field detuning, and Γ is the excited state decay rate. Often, a steady-state light shift potential, derived from the Hamiltonian (2), has been used as an effective atom-field interaction [35],

$$\frac{\hbar\Delta}{2} \ln \left[1 + \frac{8|\chi|^2 g^2(t) \cos^2(kx)}{(\Gamma/2)^2 + \Delta^2} \right]. \quad (6)$$

While this potential is important for smaller detunings and/or larger intensities, it is strictly valid only for $\Gamma\tau \gg 1$. On the other hand, the dressed state potential,

$$\frac{\hbar\Delta}{2} \sqrt{1 + 16|\chi|^2 g^2(t) \cos^2(kx) / \Delta^2}, \quad (7)$$

neglects spontaneous emission and assumes that the atom in its ground state adiabatically evolves into one of the two dressed states. For our work we follow the experimental findings of Natarajan and coworkers [6]. They show that focusing is improved by taking a short interaction time and a large detuning relative to the Rabi frequency and decay rate. In our case these conditions avoid spontaneous emission (diffusive aberration [17]) both during and after the atom-field interaction. In this limit the two potentials, Eqs. (6) and (7), reduce to the same

effective potential, ignoring spatially independent energy terms. The Hamiltonian in a field interaction representation for the ground state wave function $\psi(x, t)$ after adiabatically eliminating the excited state for $\Delta \gg 2|\chi|$ and $4\Gamma\tau|\chi|^2/\Delta^2 \ll 1$ ($\psi_e(x, t) \sim 2\chi/\Delta \simeq 0$) is

$$H = \frac{p_x^2}{2M} + \frac{2\hbar|\chi|^2}{\Delta}g^2(t)\cos(qx). \quad (8)$$

If the incident atom wave function is uniform [$\psi(x, t=0^-) = 1$], then just after a single interaction the wave function is given by

$$\psi(x, t=0^+) = \exp[i(\theta/2)\cos(qx)] \quad (9a)$$

$$= \sum_{n=-\infty}^{\infty} i^n J_n(\theta/2)e^{inqx}, \quad (9b)$$

where

$$\theta = -\left(\frac{4|\chi|^2}{\Delta}\right)\int_{-\infty}^{\infty} dtg^2(t) \quad (10)$$

is an effective pulse area for the far-detuned atom-field interaction, and J_n is a Bessel function of order n . Equation (9a) is valid in the Raman-Nath [36] or thin lens approximation, for which the $p_x^2/(2M)$ term is ignored during the interaction so that the field acts as a standing wave phase grating for the atoms. A standard condition given for the Raman-Nath approximation for thin lens focusing is [17,22]

$$|\theta|\omega_q\tau/2 \ll 1. \quad (11)$$

The two-photon recoil frequency is

$$\omega_q = \frac{\hbar q^2}{2M} = 2\pi\frac{L_T}{U}, \quad (12)$$

and $L_T = \lambda^2/(2\lambda_{dB})$ is the Talbot distance for the atom beam. The momentum eigenstates, $\exp[inqx]$, which are coherently superposed to form this wave function, each have the free particle energy $n^2\hbar\omega_q$.

A. Thin versus thick lens regimes

Before we proceed, a clarification is needed to emphasize the differences between the thin lens (Raman-Nath) and thick lens regimes of the SW atom lens. Some of the quantitative differences have been examined by Henkel and coworkers [37] in relation to Fraunhofer diffraction of atoms and from a ray optics (classical) perspective by McClelland for focusing [19]. For focusing considerations we assume square pulses, $g(t) = 1$ for $-\tau/2 \leq t \leq \tau/2$ and zero otherwise, in order to obtain quantitative results. We also require

$$\omega_q\tau \ll 1, |\theta| \gg 1. \quad (13)$$

Conditions (13) are necessary for high contrast, thin lens atom focusing, where we are interested in the atoms after propagating through the lens. (The pulse shape will affect the coefficients of our results, not the scaling with θ and $\omega_q\tau$.)

The Raman-Nath regime leading to condition (11) is normally defined as an interaction for which the average kinetic energy gained by the atoms remains much smaller than the interaction strength coupling the momentum components, $\langle p^2(t)/(2M) \rangle \ll \hbar|\chi|^2/|\Delta|$ in the square pulse case. If this condition is violated while (13) holds, the lens is thick, and the atoms can focus within the interaction region near the time $t \simeq -\tau/2 + \pi(|\chi|^2\omega_q/|\Delta|)^{-1/2}/4 < \tau/2$. If the atoms have not focused completely by the end of the pulse, they will exit the interaction region amplitude modulated. To lowest order in $\theta\omega_q\tau$, the amplitude correction which multiplies the wave function (9a) immediately after the square pulse can be calculated to be $\exp[\theta\omega_q\tau\cos(qx)/4]$.

However, the atoms also acquire an additional, spatially-modulated phase shift, $\theta^2\omega_q\tau\cos(2qx)/24$ to lowest order in $\theta^2\omega_q\tau$. This is called the WKB correction by Henkel and coworkers [37] and has its semiclassical origin in the harmonic motion of the atoms during the interaction. From a quantum perspective these amplitude and phase changes are caused simply by the kinetic energy acquired during the interaction. Heuristically, using the wave function which is evolving in the SW field, $\psi(x, t) = \exp[-i2|\chi|^2t\cos(qx)/\Delta]$, the correction which multiplies $\psi(x, \tau/2)$ can be written as

$$\exp\left[\frac{-i}{\hbar}\int_{-\tau/2}^{\tau/2} dt\psi^*(x, t)\frac{p^2}{2M}\psi(x, t)\right] = \quad (14)$$

$$\exp[\theta\omega_q\tau\cos(qx)/4 - i\omega_q\tau\theta^2(1 - \cos(2qx))/24], \quad (15)$$

giving the rigorously correct result. If we are interested in far-field diffraction, the momentum state wave function can change significantly from the spectrum of Eq. (9b) if $\theta^2\omega_q\tau/24 \gtrsim 1$ even if condition (11) is satisfied.

In the Fresnel focal region of interest here, while the spatially-dependent phase shift is crucial in determining the thin lens properties of the SW field, we require $|\theta|/2 \gg \theta^2\omega_q\tau/6$ to assure the dominance of the Raman-Nath wave function (9a) near the focus. In other words a corrected Raman-Nath condition,

$$|\theta|\omega_q\tau/3 \ll 1, \quad (16)$$

is sufficient to observe thin lens focusing, but the additional thin lens condition, $\theta^2\omega_q\tau\cos(2qx)/24 \ll 1$, may be necessary to ignore corrections to Eq. (9a) for other observables, like the far-field diffraction pattern or the time-dependent behavior of Fourier components of the density in echo configurations. Putting the results together, the corrected wave function to lowest order in $\theta^2\omega_q\tau$, $\theta\omega_q\tau$,

$$\psi(x, \tau/2) = \exp[i(\theta/2) \cos(qx)] \quad (17)$$

$$\times \exp[i\theta^2 \omega_q \tau \cos(2qx)/24] \exp[\theta \omega_q \tau \cos(qx)/4], \quad (18)$$

could be incorporated into the theoretical work below if necessary. We have verified these quantitative results using a Crank-Nicholson technique to integrate the Schrödinger equation for the far-detuned SW Hamiltonian (8) numerically on a lattice [38].

B. Results for far-detuned, thin lens focusing

Returning to Eqs. (9) as the initial condition for the free motion, since only the wave function phase has been changed during the interaction, the total atom density,

$$\rho(x, t) = |\psi(x, t)|^2 + |\psi_e(x, t)|^2 \simeq |\psi(x, t)|^2, \quad (19)$$

is initially uniform. As different Fourier components of the wave function acquire different phase shifts, $\varphi_n(t) = n^2 \omega_q t$, during the free evolution, the atom density for $t > 0$ becomes spatially modulated. The period of the spatial modulation is equal to $\lambda/2 = 2\pi/q$. Transferring to the dimensionless variables,

$$x \rightarrow qx, \quad t \rightarrow \omega_q t, \quad (20)$$

for $t > 0$ one finds [26,27]

$$\psi(x, t) = \sum_{n=-\infty}^{\infty} i^n J_n[\theta/2] e^{i(nx - n^2 t)}, \quad (21a)$$

$$\rho(x, t) = \sum_{n=-\infty}^{\infty} J_n[\theta \sin(nt)] e^{inx}. \quad (21b)$$

This result, exact in the thin lens approximation, is used below for the numerical study of atom focusing. We refer to the exact calculations by this Fourier technique as Method 1 in the text and figures that follow.

Arbitrarily precise values of the focal time t_f (giving the focal plane position for the beam, $L_f = Ut_f$) for a given θ are defined by the first maximum of the density along $x = 0$, $\rho(0, t)$, as a function of θ using Eq. (21b). Given the focal time, we can further characterize the lens by the density profile at the focus $\rho(x, t_f)$ and its peak $\rho(0, t_f)$, the spot size of the focus w , the depth of focus Δt , and the background density $\rho(\pi, t_f)$ [39]. The spot size w (HWHM of the density profile $\rho(x, t_f)$, where $\rho(0, t_f)$ is the maximum) can be defined implicitly as the smallest positive root of the equation

$$\rho(w, t_f) = 1/2 \rho(0, t_f) \quad (22)$$

Similarly, the depth of focus (confocal parameter) can be defined using Eq. (21b) as the time window,

$$\Delta t = t_+ - t_- \text{ for } t_- < t_f < t_+, \quad (23)$$

within which the density along $x = 0$ rises from half its peak value at t_- to its peak value at t_f and back again at t_+ , given implicitly by

$$\rho(0, t_{\pm}) = 1/2 \rho(0, t_f). \quad (24)$$

This region is not symmetric with respect to the focal time t_f as a result of the spherical aberration of the lens. (Note that the choice of θ as positive is unimportant even though it implies a red detuning of the field. The $\theta < 0$ case is identical but shifted in x by π .)

Several of these exact lens parameters, as calculated by Method 1, are compared to the approximate diffraction theory below. Equations (21b) will be modified to account for finite beam divergence and chromatic aberration in Sec. IV; by its nature the Fourier method includes spherical aberration (anharmonicity in the SW potential) to all orders in the lens curvature. Although Eqs. (21) are exact, they offer no transparent possibilities for obtaining analytical forms for the lens parameters as functions of θ . In contrast, a diffraction theory can be used to find approximate, asymptotic expressions ($\theta \gg 1$) for the θ -dependences of the lens parameters.

Rewriting Eq. (21a) as an integral in the coordinate representation, we can express the wave function as

$$\psi(x, t) = \int_{-\infty}^{\infty} dx' G(x - x', t - t') \psi(x', t'), \quad (25)$$

where the Fresnel-Kirchhoff propagator of the free atom motion is given in the dimensionless variables (20) by

$$G(x, t) = (4\pi i t)^{-1/2} \exp(ix^2/4t). \quad (26)$$

The integrand wave function is taken as $\psi(x', t' = 0) = \exp[i(\theta/2) \cos(x')]$. In this form we are first interested in the wave function behavior near the focal points, $x_m = 2\pi m$, for integer m and times t immediately following the interaction. The relevant time scale for focusing will become apparent shortly. When $\theta \gg 1$, the main contribution to the integral (25) near x_m at these times arises from small values of $|x' - x_m|$, where the potential in Eq. (8) is nearly harmonic. We choose to expand around the point $x' = 0$ ($m = 0$) and downplay the periodicity of the wave function for the diffraction theory. Replacing $\cos(x')$ by $1 - x'^2/2$, the atom density at the center,

$$\rho(0, t) \simeq (1 - t\theta)^{-1}, \quad (27)$$

contains a singularity at $t = \theta^{-1}$ which determines the approximate position of the focal plane.

To obtain a finite value for the atomic density, spherical aberration (*i.e.*, anharmonic terms in the potential) must be considered. Expanding $\cos(x')$ to the x'^4 term, omitting the phase factor $\exp(ix'^2/4t)$, and choosing the scaled position $\xi = 1/2(\theta/3)^{1/4} x'$ as an integration variable, we find that the asymptotic wave function in the vicinity of $x = 0$ is

$$\psi(x, t) \sim (3/\theta)^{1/4} (\pi it)^{-1/2} \exp(i\theta/2) f(\tilde{x}, \tilde{\omega}), \quad (28a)$$

$$f(\tilde{x}, \tilde{\omega}) = \int_{-\infty}^{\infty} d\xi \exp(-i\tilde{x}\xi + i\tilde{\omega}\xi^2 + i\xi^4), \quad (28b)$$

$$\tilde{x} = (3/\theta)^{1/4} x/t, \quad (28c)$$

$$\tilde{\omega} = (3/\theta)^{1/2} (t^{-1} - \theta). \quad (28d)$$

The main contribution to the wave function comes from the region where the integrand phase originating from the anharmonic term is of the order of unity ($|\xi_{\max}| \sim 1$ or $|x'_{\max}| \sim \theta^{-1/4}$). To determine the validity of Eqs. (28), the next anharmonic term ($\sim x'^6$) must produce a small addition to the integrand phase in this region, implying $\theta x'^6_{\max} \ll 1$, or

$$\theta^{-1/2} \ll 1. \quad (29)$$

This condition defines the proper asymptotic limit - a wave function correction of relative weight $\theta^{-1/2}$ in Eq. (28a) could be included to increase the calculation's accuracy. We assume condition (29) holds.

>From Eqs. (28) the time-dependent density,

$$\rho(x, t) = |\psi(x, t)|^2 \sim (3/\theta)^{1/2} (\pi t)^{-1} F(\tilde{x}, \tilde{\omega}) \quad (30a)$$

$$F(\tilde{x}, \tilde{\omega}) = |f(\tilde{x}, \tilde{\omega})|^2, \quad (30b)$$

contains both the slowly-varying t^{-1} dependence and the sharp dependence of $F(\tilde{x}, \tilde{\omega})$ in the vicinity of $t = \theta^{-1}$. At the focal center ($\tilde{x} = 0$), the integral (28b) can be expressed analytically (see Ref. [40], No. 3.696) through fractional Bessel functions as

$$f(0, \tilde{\omega}) = 2^{-3/2} \pi |\tilde{\omega}|^{1/2} \exp[-i(\tilde{\omega}^2 - \pi)/8] \times \left[J_{-1/4}(\tilde{\omega}^2/8) + i^{3/2} \text{sign}(\tilde{\omega}) J_{1/4}(\tilde{\omega}^2/8) \right], \quad (31)$$

giving an analytical asymptotic expression for the density as a function of time along $x = 0$,

$$\rho(0, t) \sim (3/\theta)^{1/2} (\pi t)^{-1} |f(0, \tilde{\omega})|^2. \quad (32)$$

The lens parameters in this asymptotic diffraction theory are defined in the same way as they were for the exact Fourier theory above. They are found graphically or numerically by evaluating Eqs. (28), (30), and (32). The focal time t_f for a given θ (which is not given by $t = \theta^{-1}$) can be found as the first maximum of $\rho(0, t)$ from Eq. (32). Using this focal time t_f , we further characterize the SW lens by the peak density $\rho(0, t_f)$ evaluating Eq. (32), by the density profile at the focus $\rho(x, t_f)$ found from Eqs. (28) and (30), by the spot size w (HWHM of the density profile $\rho(x, t_f)$), and by the depth of focus Δt found from Eqs. (30a) and (32).

Calculations performed with these asymptotic diffraction results, only restricting x to be near $x_m = 2\pi m$, are referred to as Method 2. In addition to the Method 2 asymptotic results, we can derive expressions which are

valid both for $x \simeq x_m$ and for the time restricted to be near the focus, $t \simeq \theta^{-1}$, namely within the depth of focus. This further approximation, which is referred to as Method 3, leads to analytical expressions for the lens parameters in the asymptotic limit.

In order to proceed, we need to determine the peak of the function $F(0, \tilde{\omega})/t$ from Eq. (30a) near $t \simeq \theta^{-1}$ for $\theta^{1/2} \gg 1$. First, times within the depth of focus $|t - \theta^{-1}|$ are roughly determined by the requirement $|\tilde{\omega}| \sim 1$ or

$$|t - \theta^{-1}| \sim \theta^{-3/2} \quad (33)$$

and scale as $\sim \theta^{-1/2}$ times the focal plane position. For $\theta^{1/2} \gg 1$, Eq. (33) justifies the inequality

$$|t - \theta^{-1}| \ll t. \quad (34)$$

Therefore, it is sufficient to replace the slowly-varying time dependence t^{-1} by θ in Eqs. (28c) and (30a), taking the lowest order limit of (28d) near $t \simeq \theta^{-1}$. In other words we replace Eqs. (28c) and (28d) by

$$\tilde{x}_a \sim 3^{1/4} \theta^{3/4} x \text{ and} \quad (35a)$$

$$\tilde{\omega}_a \sim 3^{1/2} \theta^{3/2} (\theta^{-1} - t), \quad (35b)$$

respectively, to arrive at the density near the focus,

$$\rho(x, t) \sim 3^{1/2} \pi^{-1} \theta^{1/2} F[\tilde{x}_a, \tilde{\omega}_a]. \quad (36)$$

The subscript a reminds us these results are asymptotic. Equation (36) can be evaluated numerically. Unlike Eqs. (30a) and (32), Eq. (36) is independent of an explicit dependence on t and, therefore, is a universal (scaled) density function. Inserting Eqs. (31) and (35b) into (36), one finds that the asymptotic time evolution of the density along $x = 0$ can be written analytically as

$$\rho(0, t) \sim 2^{-3} (3\theta)^{1/2} \pi |\tilde{\omega}_a| \quad (37)$$

$$\times \left| J_{-1/4}(\tilde{\omega}_a^2/8) + i^{3/2} \text{sign}(\tilde{\omega}_a) J_{1/4}(\tilde{\omega}_a^2/8) \right|^2 \quad (38)$$

and is shown in Fig. 1.

Approximate expressions for the focal parameters are derived by finding the maximum of the function $F(0, \tilde{\omega}_a) = |f(0, \tilde{\omega}_a)|^2$ either numerically using Eq. (37) or graphically from Fig. 1. We find that the maximum $F(0, \tilde{\omega}_f) \approx 6.94$ occurs at $\tilde{\omega}_f \approx -2.20$. Hence, the asymptotic focal time is given by inverting Eq. (35b),

$$t_f \sim \theta^{-1} \left[1 - \tilde{\omega}_f (3\theta)^{-1/2} \right] \simeq \theta^{-1} \left[1 + 1.27\theta^{-1/2} \right]. \quad (39)$$

The asymptotic atom distribution at the focal plane, $\rho(x, t_f)$, putting $\tilde{\omega}_a = \tilde{\omega}_f$ into Eq. (36), is also plotted in Fig. 1. For the peak density we have

$$\rho(0, t_f) \sim 3^{1/2} \pi^{-1} F(0, \tilde{\omega}_f) \theta^{1/2} \simeq 3.83\theta^{1/2}. \quad (40)$$

The asymptotic focal spot size w can be expressed through the half-width \tilde{x}_f of the function $F(\tilde{x}_a, \tilde{\omega}_f)$,

which is found to be $\tilde{x}_f \approx 0.979$. Inverting Eq. (35a) gives the expression

$$w \sim 3^{-1/4} \tilde{x}_f \theta^{-3/4} \simeq 0.744 \theta^{-3/4}. \quad (41)$$

The asymptotic depth of focus, Δt , defined by Eqs. (23) and (24), is evaluated using Eq. (37) by finding the two values $\tilde{\omega}_\pm$ on either side of $\tilde{\omega}_f \approx -2.20$ for which $F(0, \tilde{\omega}_\pm) = F(0, \tilde{\omega}_f)/2 \approx 3.47$. These are $\tilde{\omega}_+ \approx -3.42$ and $\tilde{\omega}_- \approx -0.115$, giving a depth of focus from inverting Eq. (35b) of

$$\Delta t \sim -3^{-1/2} (\tilde{\omega}_+ - \tilde{\omega}_-) \theta^{-3/2} \simeq 1.91 \theta^{-3/2}. \quad (42)$$

Equations (35)-(42) constitute the Method 3 results describing the SW lens near $x = 2\pi m$ and $t = \theta^{-1}$.

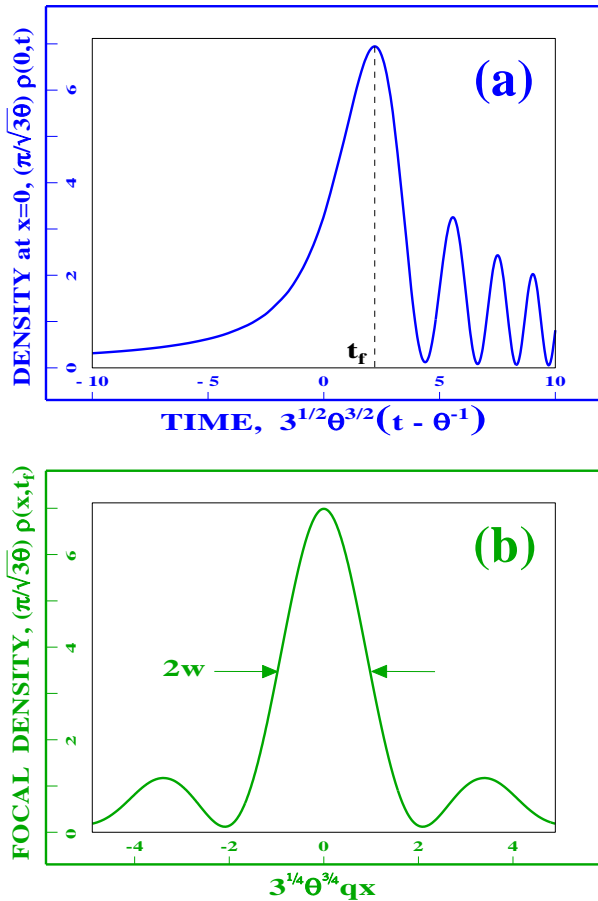


FIG. 1. Scaled asymptotic (as $\theta \rightarrow \infty$) atom densities in far-detuned focusing. (a) Time evolution of the atom density at $x = 0$, $\rho(0, t)$. (b) Density profile at the focal plane, $\rho(x, t_f)$. Time zero in the graph corresponds to the focal point in the harmonic approximation.

In much the same way, we can use Methods 2 and 3 to derive expressions for the background density, defined as the density $\rho(x_b, t)$ at the midpoints between periodic focuses, $x_b = x_m + \pi$. We need to find the wave function, Eq. (25), at the point $x_b = \pi$. Since no singularity arises in the integral for $t \lesssim t_f$ when the integrand is expanded

around $x' = \pi$, only the harmonic term is needed to find the wave function, where $\cos(x') \simeq (x' - \pi)^2/2 - 1$. We find the approximate wave function, $\sim (1 + t\theta)^{-1/2}$, and background density,

$$\rho(\pi, t) \sim (1 + t\theta)^{-1}, \quad (43)$$

correct to order θ^{-2} . This is the Method 2 result. This expression allows us to find the asymptotic density contrast of importance for lithography, $c(t)$. The contrast is defined [7] to be the ratio of the atomic density at the focal points x_m to the background,

$$c(t) = \rho(0, t) / \rho(\pi, t), \quad (44)$$

where $\rho(0, t)$ is given by Eqs. (31) and (32) for Method 2.

In addition, putting the asymptotic focal time (39) from Method 3 into Eq. (43), the asymptotic background density at the focus is $\rho(\pi, t_f) \sim (1 + t_f \theta)^{-1}$, or

$$\rho(\pi, t_f) \sim 0.5(1 - 0.635\theta^{-1/2}). \quad (45)$$

From Eq. (44) the asymptotic contrast ratio at the focus is (within the accuracy of this calculation)

$$c(t_f) = \frac{\rho(0, t_f)}{\rho(\pi, t_f)} \sim 7.66\theta^{1/2}. \quad (46)$$

Equations (45) and (46) are a Method 3 result.

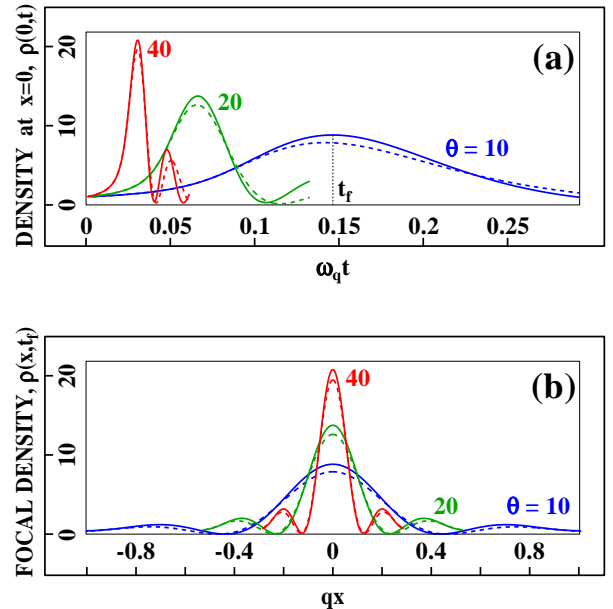


FIG. 2. Far-detuned focusing. Comparison between exact densities by the Fourier method (Method 1, solid lines) and approximate asymptotic densities near $x = 0$ (Method 2, dashed lines) for different values of the pulse area θ . (a) Time evolution of the atom density at $x = 0$, $\rho(0, t)$. (b) Density profile at the focal plane, $\rho(x, t_f)$.

To summarize, we now have three methods to find the lens parameters, each with different levels of numerical effort required to use it. The relevant equations for these methods are listed in Table 1:

Table 1. Techniques and equations for three different methods of calculating thin SW lens parameters. The numbers in the Table correspond to equations in the text.

Method	Numerical Sum	Numerical Integral	Analytical Expression
1. Exact Fourier	21b		
Asymptotic			
2. $ x - m\pi \ll 1$ $t > 0$		30	32 43
Asymptotic			
3. $ x - m\pi \ll 1$ $t \sim \theta^{-1}$		36	37-42 45-46

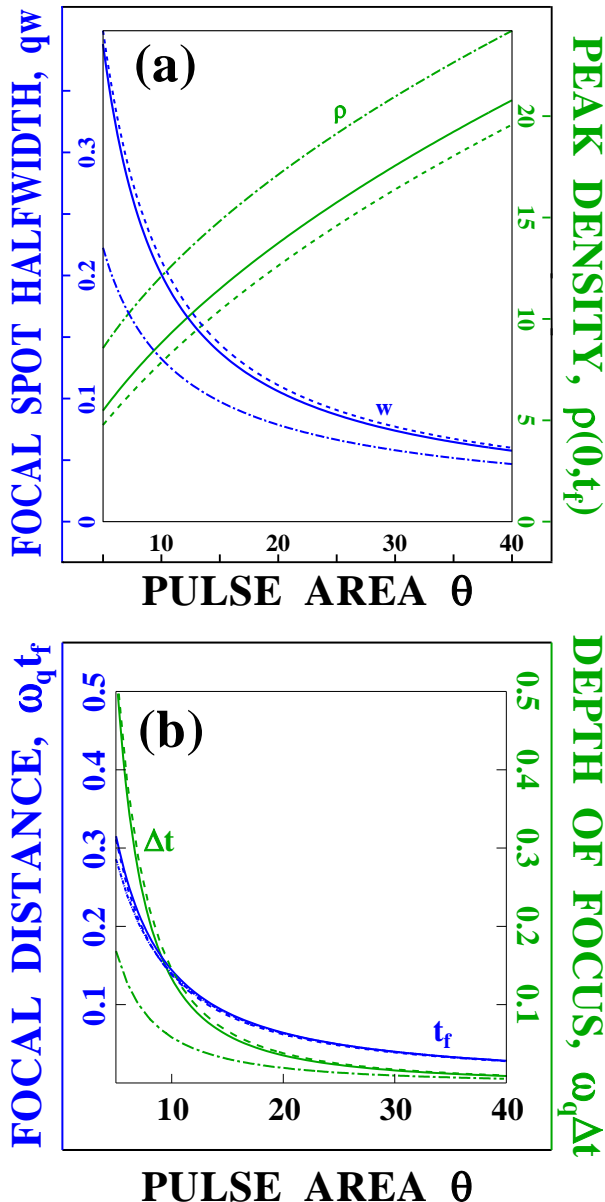


FIG. 3. Pulse area dependences of the lens parameters in far-detuned focusing: (a) Peak focal densities $\rho(0, t_f)$ (curves ρ) and spot sizes w (HWHM of the density profiles at the focal planes). (b) Focal distances t_f and depths of focus Δt . Computational methods: 1. Exact Fourier (solid), 2. Asymptotic diffraction near $x = 0$ (dashed), 3. Asymptotic diffraction near $x = 0$ and $t = \theta^{-1}$ (dot-dashed). Note that the three methods give almost identical result for t_f .

In Fig. 2 the exact atom density at the center $\rho(0, t)$ and atom distribution at the focal plane $\rho(x, t_f)$, as calculated by Method 1, are compared with the approximate expressions from Method 2. The convergence of the Method 2 result as θ increases is evident. In Figs. 3 the pulse area dependences of the focal parameters, as calculated by the three methods, are compared. The accuracy of Method 2 is generally better than that of Method 3, but all methods converge for $\theta^{1/2} \gg 1$. These results are discussed further in Sec. V, including the easily explained, constant offsets of the asymptotic peak densities in Fig. 3a.

III. RESONANT FOCUSING

We now consider the density modulation and focusing caused by a resonant standing wave field acting on a two-level atom. If the pulse duration satisfies the inequality

$$\tau \ll \min\{(\omega_k \theta)^{-1}, |\Delta|^{-1}, \Gamma^{-1}\}, \quad (47)$$

[the field area θ for a resonant SW field is defined below by Eq. (50)], then during the interaction the ground and excited state wave functions, $\psi(x, t)$ and $\psi_e(x, t)$, evolve in an interaction representation according to

$$\dot{\psi}(x, t) = -2i\chi g(t) \cos(kx) \psi_e(x, t) \quad (48a)$$

$$\dot{\psi}_e(x, t) = -2i\chi g(t) \cos(kx) \psi(x, t). \quad (48b)$$

By satisfying Eq. (47), we are assured that the resonant atom-field interaction is in the Raman-Nath regime and that the pulse duration is shorter than the excited state lifetime, avoiding the complications of saturation and momentum space diffusion. If before the interaction the incident wave function is uniform in the ground state, $\psi(x, 0^-) = 1$, then just after the interaction

$$\begin{pmatrix} \psi_e(x, 0^+) \\ \psi(x, 0^+) \end{pmatrix} = \begin{pmatrix} -i \sin[(\theta/2) \cos(kx)] \\ \cos[(\theta/2) \cos(kx)] \end{pmatrix}, \quad (49)$$

where the effective pulse area for the resonant atom-field interaction is defined as

$$\theta = 4\chi \int_{-\infty}^{\infty} dt g(t). \quad (50)$$

The subsequent free space evolution and radiative decay of the system were recently analyzed [28] using the Fourier method for the closed two-level scheme (*i.e.*, the

excited state $|e\rangle$ decays only to $|g\rangle$) [41]. However, the results that are relevant to the problem discussed here pertain to any excited state decay scheme. In the following paragraphs we summarize these results in order to apply the three methods of Sec. II to the resonant case. Our goal is to separate two terms in the free evolution of the ground state: (1) the strict Hamiltonian evolution, resulting from the ground state amplitude produced coherently by the SW pulse, and (2) the terms which result from spontaneous decay of the excited state. Such a separation is straightforward by the Fourier technique, Method 1. Once this is done, we can use a diffraction analysis to obtain asymptotic results for the focal density caused by the Hamiltonian term, $\psi(x, 0^+)$ in Eq. (49). The diffraction analysis, Methods 2 and 3 from above, leads to analytic expressions for the resonant SW lens parameters and, anticipating the results, sheds light on the Rabi-like oscillation of the lens parameters as a function of θ .

After the excited state decays (in a time $t \gtrsim \Gamma^{-1}$ following the pulse), the total atomic density $\rho(x, t)$ involves only the ground state and is a periodic function of x having period $\lambda/2$. The atomic system can no longer be described simply by a wave function since we must trace the full density matrix over the spontaneously emitted photons to form the reduced density matrix $\rho(x, x', t)$. However, the part of the density matrix which was produced coherently by the pulse can still be described by evolving the wave function $\psi(x, 0^+)$ in Eq. (49) into $\psi(x, t)$. This was done in Ref. [28]. The total density $\rho(x, t)$, which is formally the diagonal component $\rho(x, x, t)$ of the reduced density matrix, can be expanded in a set of Fourier components,

$$\begin{aligned} \rho(x, t) &= \sum_{n=-\infty}^{\infty} \left[\rho_n^{(S)}(t) + \rho_n^{(D)}(t) \right] e^{inqx} \\ &= \rho^{(S)}(x, t) + \rho^{(D)}(x, t) \end{aligned} \quad (51a)$$

$$\rho^{(S)}(x, t) = \sum_{n=-\infty}^{\infty} \rho_n^{(S)}(t) e^{inqx} \quad (51b)$$

$$\rho^{(D)}(x, t) = \sum_{n=-\infty}^{\infty} \rho_n^{(D)}(t) e^{inqx}. \quad (51c)$$

Each ground state Fourier component, $\rho_n(t) = \rho_n^{(S)}(t) + \rho_n^{(D)}(t)$, consists of two terms: a stimulated term, $\rho_n^{(S)}(t)$, caused by the free evolution of $\psi(x, 0^+)$, and a spontaneous term, $\rho_n^{(D)}(t)$.

After Fourier expansion of $\psi(x, 0^+)$, the stimulated Fourier components of the density are given by squaring

$$\psi(x, t) = \sum_{n=-\infty}^{\infty} (-1)^n J_{2n}(\theta/2) e^{inqx - in^2\omega_q t}. \quad (52)$$

to form [28]

$$\begin{aligned} \rho_n^{(S)}(t) &= 1/2 \{ J_{2n}[\theta \sin(n\omega_q t/2)] \\ &\quad + (-1)^n J_{2n}[\theta \cos(n\omega_q t/2)] \}. \end{aligned} \quad (53)$$

In particular, the average stimulated density ($n = 0$) is

$$\rho_0^{(S)}(t) = 1/2 [1 + J_0(\theta)]. \quad (54)$$

Each of the stimulated terms, $\rho_n^{(S)}(t)$, is periodic in time with the Talbot period, $T = 2\pi/\omega_q$.

The n th spontaneous term, $\rho_n^{(D)}(t)$, results directly from the decay of the n th Fourier component of the excited state population. Since this decay is accompanied by an atomic recoil, each harmonic's spontaneous term for $n \neq 0$ acquires an additional Doppler phase which depends on the momentum $\hbar\mathbf{k}_r$ of the emitted photon, $n\hbar q\hat{\mathbf{x}} \cdot \mathbf{k}_r t/M$. The resulting inhomogeneous dephasing after integrating over spontaneous emission directions leads to a decay of the spontaneous part of the $n \neq 0$ Fourier components on a time scale of the order of T ,

$$\rho_{n \neq 0}^{(D)}(t \gg T) \rightarrow 0. \quad (55)$$

In the spatial domain this is equivalent to a length scale on the order of the Talbot distance, L_T . While we could use the complete results of Ref. [28] to analyze focusing including this spontaneous term for times $t \lesssim T$, we choose instead to simplify the problem by waiting exactly j Talbot periods ($t \simeq jT \gg T$), where j is a positive integer greater than one. As a result, one can neglect $\rho_{n \neq 0}^{(D)}(t)$ in Eqs. (51).

The $n = 0$ spontaneous Fourier component does not decay. For $n = 0$ it follows from the Fourier expansion of $\psi_e(x, 0^+)$, for example, that

$$\rho_0^{(D)}(t) = 1/2 [1 - J_0(\theta)]. \quad (56)$$

Thus, in accordance with the conservation of probability, the total average density is one by summing Eqs. (54) and (56),

$$\rho_0(t) = \rho_0^{(S)}(t) + \rho_0^{(D)}(t) = 1. \quad (57)$$

Combining these results, the total density is

$$\rho(x, t \gg T) = 1 + \sum_{n \neq 0} \rho_n^{(S)}(t) e^{inqx}. \quad (58)$$

We can now use Eqs. (51), (53), (56), and (58) as exact, Method 1 expressions to compare to an approximate diffraction theory.

To present a diffraction theory of resonant focusing, we consider only the stimulated ground state wave function $\psi(x, t)$ evolving from $\psi(x, jT + 0^+) = \psi(x, 0^+)$ [Eq. (49)], remembering that it is first necessary to add an integer number of Talbot periods, jT , to reach an "initial" time when the modulated spontaneous contribution

can be neglected. Moreover, we must add on the additional background density from the spontaneous term, Eq. (56), to the final result.

The wave function, $\psi(x, 0^+) = \cos[(\theta/2) \cos(kx)]$, is amplitude modulated; however, $\psi(x, 0^+)$ superposes two terms, each of which is phase modulated,

$$\psi(x, 0^+) = \psi_+(x, 0^+) + \psi_-(x, 0^+), \quad (59a)$$

$$\psi_{\pm}(x, 0^+) = 1/2 \exp[\pm i(\theta/2) \cos(kx)]. \quad (59b)$$

These states can be seen as evolving independently, leading to the components of $\psi(x, t)$ we denote as $\psi_{\pm}(x, t)$. Therefore, the problem of focusing after this specific type of amplitude modulation can be mapped onto the problem of focusing by a phase grating. For times $\omega_k t \simeq \theta^{-1}$, $\theta > 0$, near the even antinodes, $kx = 0, \pm 2\pi, \dots$, the component $\psi_+(x, t)$ is responsible for focusing while the component $\psi_-(x, t)$ evolves smoothly as a background density. Near the odd antinodes, $kx = \pm\pi, \pm 3\pi, \dots$, the role of the components $\psi_{\pm}(x, t)$ is reversed. The stimulated density is then given by

$$\rho^{(S)}(x, t) = |\psi_+(x, t) + \psi_-(x, t)|^2 \quad (60)$$

and the total density, adding on the spontaneous background $\rho_0^{(D)}(t)$, by

$$\rho(x, t) = 1/2 [1 - J_0(\theta)] + \rho^{(S)}(x, t). \quad (61)$$

Consider the atom density near $x = 0$ (the even antinodes) for the development of the asymptotic theory. Since the period of the component wave functions $\psi_{\pm}(x, t)$ is twice as large as the far detuned case [compare Eqs. (9a) and (59b)], the dimensionless coordinate and time become

$$x \rightarrow kx, \quad t \rightarrow \omega_k t, \quad (62)$$

noting that $q = 2k$ and $\omega_q = 4\omega_k$. We again assume that $\theta^{1/2} \gg 1$. For the $\psi_+(x, t)$ component, free evolution in the coordinate representation including the lowest-order spherical aberration gives

$$\psi_+(x, t) = (3/\theta)^{1/4} (4\pi i t)^{-1/2} \exp(i\theta/2) f(\tilde{x}, \tilde{\omega}), \quad (63)$$

where the function f and variables $\tilde{\omega}$ and \tilde{x} are given by Eqs. (28b - 28d).

To calculate $\psi_-(x, t)$, it is sufficient to consider only the harmonic part of the potential near $x = 0$, just as we did for the background term (43) in the phase modulation case. Replacing $\psi(x', t')$ in the Fresnel-Kirchhoff equation (25) by $\psi_-(x', 0^+)$ and using the expansion $\cos(x') \approx 1 - x'^2/2$, one finds

$$\psi_-(x, t) = 1/2 (1 + \theta t)^{-1/2} \exp(-i\theta/2 + i\tilde{x}_-^2), \quad (64a)$$

$$\tilde{x}_- = [4t(1 + \theta t)]^{-1/2} x. \quad (64b)$$

This contribution remains of order unity at the focus, i.e., it has relative weight $\theta^{-1/4}$ compared to Eq. (63). Since

Eq. (63) is of higher accuracy than Eq. (64a) (relative corrections to Eq. (63) are of order $\theta^{-1/2}$), it is valid to add Eqs. (63) and (64a) to form the total wave function and calculate the density to absolute order $\theta^{1/4}$.

Interference between $\psi_+(x, t)$ and $\psi_-(x, t)$ leads to a new effect, a Rabi-like oscillation of the focused atom distribution. Squaring $\psi(x, t) = \psi_+(x, t) + \psi_-(x, t)$ to form $\rho^{(S)}(x, t)$, we find that the asymptotic stimulated atom density near $x = 0$ is

$$\begin{aligned} \rho^{(S)}(x, t) \sim (4\pi t)^{-1} (3/\theta)^{1/2} \{ & F(\tilde{x}, \tilde{\omega}) \\ & + \theta^{1/4} [2t/(1 + \theta t)]^{1/2} \\ & \times [\cos(\theta - \tilde{x}_-^2) f_c(\tilde{x}, \tilde{\omega}) \\ & - \sin(\theta - \tilde{x}_-^2) f_s(\tilde{x}, \tilde{\omega})] \}, \quad (65a) \end{aligned}$$

$$f_c(\tilde{x}, \tilde{\omega}) + i f_s(\tilde{x}, \tilde{\omega}) \equiv (2\pi/i)^{1/2} 3^{-1/4} f(\tilde{x}, \tilde{\omega}). \quad (65b)$$

Due to the symmetry between ψ_+ and ψ_- , this is the density near the focus at both the even and odd antinodes, giving a total density of spatial period $2\pi/q = \lambda/2$. Equations (65) are the Method 2 result for the resonant lens. After accounting for the relevant coordinate and time scales (62), the dominant term, $|\psi_+|^2$, looks exactly like the far detuned result of Sec. II and leads to the same lens parameters if taken alone. The interference term has a relative amplitude $\theta^{-1/4}$ near the focus ($t \simeq \theta^{-1}$) when compared to the $|\psi_+|^2$ term and oscillates sinusoidally with θ .

Now we employ Method 3, the limit of this asymptotic result for $t \simeq \theta^{-1}$. Considering the interference term as a small correction to $|\psi_+|^2$, we apply the far detuned results [Eqs. (36) and (37), $\tilde{\omega}_f \approx -2.20$, and $\tilde{x}_f \approx 0.979$] and Taylor expand Eqs. (65) around $\tilde{\omega}_f$ and \tilde{x}_f . The following asymptotic expressions can be derived for the focal parameters:

$$\begin{aligned} t_f \sim \theta^{-1} \{ & 1 - \tilde{\omega} (3\theta)^{-1/2} + 3^{-1/2} \theta^{-3/4} \\ & \times [\partial^2 F(0, \tilde{\omega}) / \partial \tilde{\omega}^2]^{-1} [\cos(\theta) \\ & \times \partial f_c(0, \tilde{\omega}) / \partial \tilde{\omega} \\ & - \sin(\theta) \partial f_s(0, \tilde{\omega}) / \partial \tilde{\omega}] \}_{\tilde{\omega}=\tilde{\omega}_f} \\ \simeq \theta^{-1} \{ & 1 + 1.27\theta^{-1/2} + \theta^{-3/4} \\ & \times [-0.465 \cos(\theta) \\ & + 0.110 \sin(\theta)] \}, \quad (66a) \end{aligned}$$

$$\begin{aligned} \rho^{(S)}(0, t_f) \sim & 3^{1/2} (4\pi)^{-1} \theta^{1/2} \{ F(0, \tilde{\omega}_f) \\ & + \theta^{-1/4} [\cos(\theta) f_c(0, \tilde{\omega}_f) \\ & - \sin(\theta) f_s(0, \tilde{\omega}_f)] \} \\ \simeq & 0.957\theta^{1/2} \{ 1 + \theta^{-1/4} [0.166 \cos(\theta) \\ & + 0.703 \sin(\theta)] \}, \quad (66b) \end{aligned}$$

$$w \sim 3^{-1/4} \theta^{-3/4} \{ \tilde{x}$$

$$\begin{aligned}
& +\theta^{-1/4} [\partial F(\tilde{x}, \tilde{\omega}) / \partial \tilde{x}]^{-1} \\
& \times [\cos(\theta) (1/2 f_c(0, \tilde{\omega}) - f_c(\tilde{x}, \tilde{\omega})) \\
& + (\partial f_c(0, \tilde{\omega}) / \partial \tilde{\omega}) (\partial F(\tilde{x}, \tilde{\omega}) / \partial \tilde{\omega}) \\
& \times (\partial^2 F(0, \tilde{\omega}) / \partial \tilde{x}^2)^{-1}] \\
& - (\text{the same with replacements} \\
& \cos(\theta) \rightarrow \sin(\theta), f_c \rightarrow f_s)] \Big|_{\tilde{\omega}=\tilde{\omega}_f, \tilde{x}=\tilde{x}_f} \\
& \simeq 0.744\theta^{-3/4} \left\{ 1 + \theta^{-1/4} [0.198 \cos(\theta) \right. \\
& \left. + 0.162 \sin(\theta)] \right\}. \tag{66c}
\end{aligned}$$

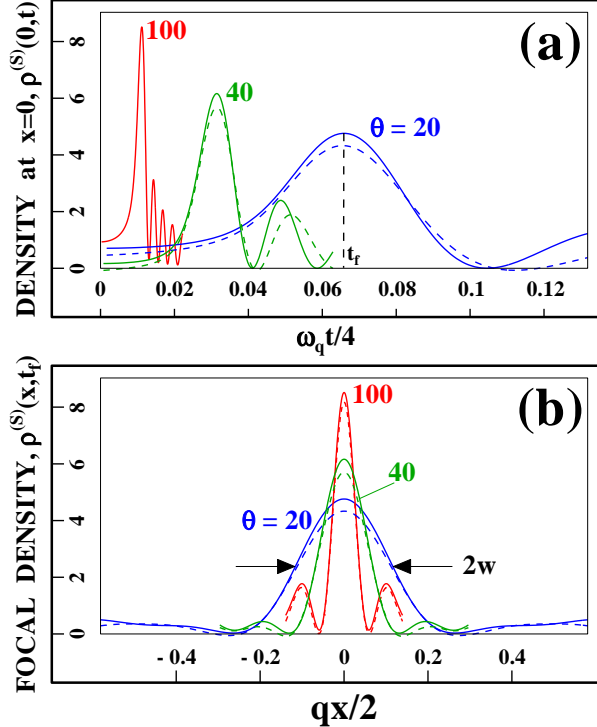


FIG. 4. Resonant focusing. Comparison between exact densities by the Fourier method (Method 1, solid lines) and approximate asymptotic densities near $x = 0$ (Method 2, dashed lines) for different values of the pulse area θ . (a) Time evolution of the atom density at $x = 0$, $\rho^{(S)}(0, t)$. (b) Density profile at the focal plane, $\rho^{(S)}(x, t_f)$. The atom density is plotted excluding the constant background term caused by spontaneous emission, $\rho_0^{(D)}(t) = (1 - J_0(\theta))/2$.

In Fig. 4 the exact time dependence of the peak stimulated density, $\rho^{(S)}(x, t)$, and the stimulated density profile at the focal plane, $\rho^{(S)}(x, t_f)$, as calculated numerically by Method 1 using Eqs. (51b) and (53) for several pulse areas, are compared with the approximate diffraction expression of Method 2, Eq. (65a). A comparison of the focal parameters as functions of the pulse area for the three different methods is plotted in Fig. 5, clearly showing the oscillation of the exact and approximate results with θ . While a diffraction theory may be unnecessary since an exact result can be calculated by the Fourier method, the physical origin of the Rabi-like term, which

is masked by the Fourier result, has been revealed by the diffraction theory to be the interference of the ψ_+ and ψ_- components of the wave function. Further discussion is again reserved for Sec. V.

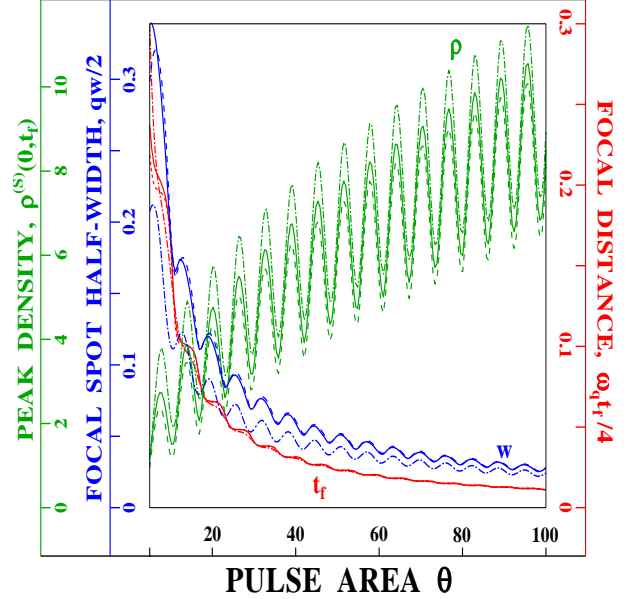


FIG. 5. Resonant focusing. Pulse area dependences of the focusing parameters: Peak focal densities [$\rho(0, t_f)$ (curves ρ)], spot sizes w (HWHM of the density profiles at the focal planes), and focal distances t_f . Computational methods: 1. Exact Fourier (solid), 2. Asymptotic diffraction near $x = 0$ (dashed), 3. Asymptotic diffraction near $x = 0$ and $t = \theta^{-1}$ (dot-dashed). The atom density is plotted excluding the constant background term caused by spontaneous emission, $\rho_0^{(D)}(t) = (1 - J_0(\theta))/2$.

IV. CHROMATIC ABERRATION AND TRANSVERSE VELOCITY DISTRIBUTIONS

A. Chromatic aberration

Chromatic aberration, the dispersion θ or wave length dependence of a lens' properties, results from a finite distribution of longitudinal velocities (*i.e.*, de Broglie wave lengths) in an atom beam. In trap experiments this type of aberration is avoided. However, for beam experiments detected in the laboratory frame, the atomic distribution would be probed or deposited at a certain distance from the interaction region, $L = Ut$. As a result, the total atom density at L will be an average of each velocity's density at L over the flux of atoms with that velocity. In general, to calculate the density, we must know the longitudinal velocity distribution or at least its statistical properties. Previous theoretical and experimental

publications that have discussed chromatic aberration in the context of atom optical lenses have used heuristic, numerical, or Monte Carlo simulation approaches [6–8,11,15,17,19]. We attack the problem from a different perspective, based on averaging the exact Fourier components over the atomic flux distribution. The technique is easy to apply, the results are simple to understand, and the conclusions have a physical interpretation.

For the remainder of the paper, the *ideal* case will refer to the monovelocity atomic beam with longitudinal velocity U and infinitely narrow longitudinal and transverse velocity distributions. In the previous sections we have presented a full characterization of the thin SW lens acting on the ideal beam. Two types of beams with more realistic longitudinal distributions are typical and will be considered here, (1) a velocity narrowed beam centered around some average velocity U_0 or (2) a thermal beam with average speed U_0 . In this section we consider only focusing by the far-detuned standing wave. For this type of lens, the exact expression for the density, Eq. (21b), can be averaged over the proper flux distribution function for a specified L by numerical integration, provided the paraxial approximation still holds: $\lambda_{dB,0} = 2\pi\hbar/(MU_0) \ll \lambda$. In addition, the narrow velocity distribution case allows for an approximate analytical solution to compare to the numerically integrated result: by expanding the lens parameters around the average values of the flux distribution, we can account for chromatic aberration analytically using the density of the Fourier method.

In the laboratory frame the atoms interact with a SW field with a fixed width σ_z along the z direction and are then detected at a fixed distance L from the lens. As a result, the pulse area θ and the time of free flight t after the lens depend on the atomic longitudinal velocity U as U^{-1} . The atomic density is defined as an average over the single-particle atomic flux distribution $W(U)$. This distribution is a measure of the probability, $W(U)dU$, to find an atom with velocity between U and $U+dU$ passing through a plane perpendicular to the z axis. (One would divide $W(U)$ by the atomic spatial density to get a true flux distribution in inverse units of particles per unit time per unit area.) To derive quantitative results, we need to specify $W(U)$ for a given experiment.

In this section we denote flux averages $\langle \rangle$ by

$$\langle F(U) \rangle = \int_0^\infty dU F(U) W(U), \quad (67)$$

taking into account that only atoms having positive velocity, $U > 0$, have to be included. Using this definition, the average velocity U_0 , the (dimensionless) relative velocity u , and the (dimensionless) flux width v are given, respectively, as

$$U_0 = \langle U \rangle, \quad (68a)$$

$$u = (U - U_0)/U_0, \quad (68b)$$

$$v = [2 \langle u^2 \rangle]^{1/2}. \quad (68c)$$

The pulse area θ and the time of flight t for each velocity class U can be defined by reference to the average velocity U_0 ,

$$\theta = \theta_0 U_0/U = \theta_0/(1+u) \text{ and } t = t_0 U_0/U = t_0/(1+u), \quad (69)$$

where $\theta_0 \simeq (-4|\chi|^2/\Delta)(\sigma_z/U_0)$ and $t_0 = L/U_0$ would be computed using U_0 . The exact, flux-averaged density $\bar{\rho}(x, t_0)$ follows immediately from Eq. (21b),

$$\begin{aligned} \bar{\rho}(x, t_0) &= \langle \rho(x, t) \rangle \\ &= \sum_{n=-\infty}^{\infty} e^{inx} \int_0^\infty dU W(U) \\ &\quad \times J_n[(\theta_0 U_0/U) \sin(nt_0 U_0/U)]. \end{aligned} \quad (70)$$

The integrals can be evaluated numerically, term-by-term, giving the flux-averaged Fourier components of the density. If the distribution $W(U)$ has a non-zero width v , then the focusing by the SW lens is degraded. We show this graphically below.

We start with the narrow velocity distribution case,

$$v \ll 1, \quad (71)$$

and derive approximate, analytical expressions from Eq. (70) to compare to an exact numerical integration. Our goal is to determine the effect of a flux width v on the focus when compared to the ideal beam results ($v \rightarrow 0$). Since $v \ll 1$, we can expand the field area and time, Eq. (69), as

$$\theta \approx \theta_0 (1 - u + u^2), \quad t \approx t_0 (1 - u + u^2). \quad (72)$$

Substituting values (72) into $\rho(x, t)$ of Eq. (21b), expanding in powers of u , and applying Eqs. (70) and (68), one finds to order v^2 that

$$\bar{\rho}(x, t_0) \simeq \rho(x, t_0) + v^2 \rho_1(x, t_0), \quad (73a)$$

$$\begin{aligned} \rho_1(x, t) &= 1/4 \sum_{n=-\infty}^{\infty} \left\{ \theta_0 [4nt \cos(nt) + (2 - (nt)^2) \right. \\ &\quad \times \sin(nt)] J'_n[\theta_0 \sin(nt)] + \theta_0^2 [\sin(nt) \\ &\quad \left. + nt \cos(nt)]^2 J''_n[\theta_0 \sin(nt)] \right\} e^{inx}, \end{aligned} \quad (73b)$$

where $\rho_1(x, t_0)$ is the lowest-order correction to the density at L as a result of the flux distribution.

To order v^2 , four of the focal parameters (the focal distance t_f , defined as the first maximum of the function $\bar{\rho}(0, t_0)$, the peak density $\bar{\rho}(0, t_f)$, the spot size w , defined as the lowest root of the equation $\bar{\rho}(w, t_f) = \bar{\rho}(0, t_f)/2$, and the depth of focus Δt , defined by $\bar{\rho}(0, t_\pm) = \bar{\rho}(0, t_f)/2$), are given by

$$t_f \simeq t_{0,f} + v^2 t_1, \quad (74a)$$

$$t_1 = - \left[\frac{\partial \rho_1(0, t) / \partial t}{\partial^2 \rho(0, t) / \partial t^2} \right]_{t=t_{0,f}}; \quad (74b)$$

$$\bar{\rho}(0, t_f) \simeq \rho(0, t_{0,f}) + v^2 \rho_1(0, t_{0,f}); \quad (74c)$$

$$w \simeq w_0 + v^2 w_1, \quad (74d)$$

$$w_1 = \left\{ \left[\frac{\partial \rho(w, t)}{\partial w} \right]^{-1} \left[\frac{1}{2} \rho_1(0, t) - \rho_1(w, t) - t_1 \frac{\partial \rho(w, t)}{\partial t} \right] \right\}_{t=t_{0,f}, w=w_0}, \quad (74e)$$

$$\Delta t = \Delta t_0 + v^2 \Delta t_1, \quad (74f)$$

$$\Delta t_1 = \frac{\frac{1}{2} \rho_1(0, t_{0,+}) - \rho_1(0, t_{0,+})}{\left[\frac{\partial \rho(0, t)}{\partial t} \right]_{t=t_{0,+}}} - \frac{\frac{1}{2} \rho_1(0, t_{0,f}) - \rho_1(0, t_{0,-})}{\left[\frac{\partial \rho(0, t)}{\partial t} \right]_{t=t_{0,-}}}, \quad (74g)$$

where $t_{0,f}$, w_0 , and $\Delta t_0 = t_{0,+} - t_{0,-}$ are the focal distance, focal spot size, and the depth of focus, respectively, for θ_0 as calculated in Sec. II for the monovelocity beam. It is significant that Eqs. (73) and (74) depend only on the dimensionless flux width v and not on the exact form of the distribution $W(U)$. The pulse area dependences of the correction coefficients, t_1 , $\rho_1(0, t_{0,f})$, and w_1 , are shown in Fig. 6. To verify Eqs. (73) and (74) for small v , we can now quantitatively compare the approximate expressions to the exact, numerically averaged density, Eq. (70), for a physically reasonable and mathematically convenient distribution function.

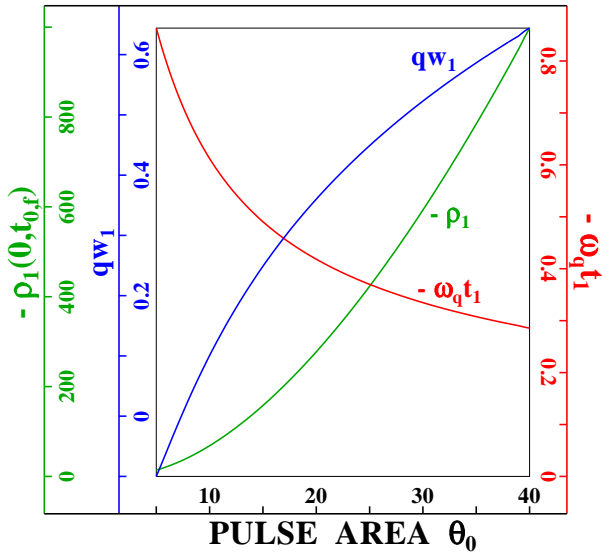


FIG. 6. Chromatic aberration for focusing atomic beams. Correction coefficients, given in Eqs. (74), as functions of the pulse area θ_0 , assuming a narrow longitudinal flux distribution, $v \ll 1$: Peak focal density $\rho_1(t_{0,f})$, focal distance t_1 , and spot size w_1 corrections. These coefficients multiply v^2 to form the lowest-order corrections to the lens parameters.

For example, we can find the flux distribution $W_{IM}(U)$ corresponding to the local Maxwellian velocity distribu-

tion,

$$W_{IM'}(U) = \frac{1}{\sqrt{\pi}V} \exp \left[- \left(U - \tilde{U}_0 \right)^2 / V^2 \right]. \quad (75)$$

The flux distribution, average velocity, and (dimensionless) flux width that follow from $W_{IM'}(U)$ can be written with accuracy $\exp(-\tilde{U}_0^2/V^2)$ as

$$W_{IM}(U) = \frac{U}{\sqrt{\pi} \tilde{U}_0 V} \exp \left[- \left(U - \tilde{U}_0 \right)^2 / V^2 \right], \quad (76a)$$

$$U_0 = \tilde{U}_0 \left(1 + V^2 / 2 \tilde{U}_0^2 \right), \quad (76b)$$

$$v = \frac{V}{\tilde{U}_0} \frac{\sqrt{1 - V^2 / 2 \tilde{U}_0^2}}{1 + V^2 / 2 \tilde{U}_0^2}. \quad (76c)$$

As long as $V/\tilde{U}_0 \ll 1$, we can be assured that $v \ll 1$. Distribution (76a) can be inserted into Eq. (70) for $\bar{\rho}(x, t_0)$, and the exact density can be evaluated at the time $t_{0,f}$ for different values of the distribution width v using the parametrization of Eq. (76c). Alternatively, the precise, flux-averaged focal time, $t_f = L_f/U_0 \neq t_{0,f}$, can be found numerically from the first maximum of $\bar{\rho}(0, t_0)$ in time and used to evaluate the density and lens parameters. The peak reduction and spot size increase for two pulse areas at $t_{0,f}$ are plotted as a function of v in Fig. 7. In Fig. 8 the density profile at the true focus, $\bar{\rho}(x, t_f)$, for one of these pulse areas is shown with and without chromatic aberration. Both figures are explained in detail in Sec. V.

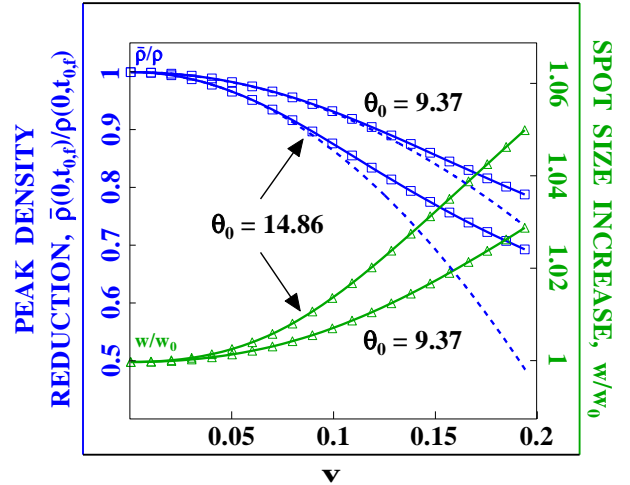


FIG. 7. Narrow longitudinal flux distribution in atomic focusing. Exact reduction in the peak focal density, $\bar{\rho}(0, t_{0,f})/\rho(0, t_{0,f})$ (boxes), and exact increase in the spot size, w/w_0 (triangles), as functions of the longitudinal flux width v for the flux distribution $W_{IM}(U)$ and for two pulse areas, $\theta_0 = 9.37$ and 14.86 . These pulse areas would produce spot sizes of 10 nm and 6.5 nm , respectively, in Na for $v = 0$. The dashed curve for $\bar{\rho}(0, t_{0,f})/\rho(0, t_{0,f})$ is the approximate, analytical dependence for small v from Eq. (74c) or Fig. 6.

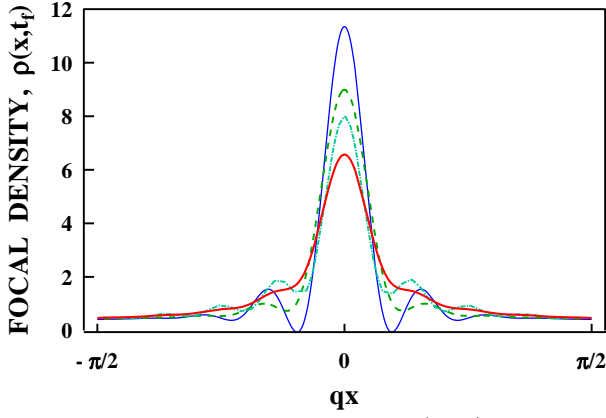


FIG. 8. Exact focal density profiles, $\rho(x, t_f)$, in the range $|qx| \leq \pi/2$ for $\theta_0 = 14.86$ with and/or without the effects of both chromatic aberration and angular divergence. The ideal atomic beam - $v = 0$, $V_x = 0$ - gives a spot size of $qw = 0.139$, or 6.5 nm in sodium (thin solid line). Pure chromatic aberration, $W_{LM}(U)$ longitudinal flux distribution - $v = 0.194$ and $V_2 = 0$ (dotted line). Pure angular divergence, P_2 (Maxwellian) transverse velocity distribution - $v = 0$ and $V_2 = 1$ (dashed line). Combined chromatic aberration and angular divergence - $v = 0.194$ and $V_2 = 1$ (thick solid line). The transverse width, $V_2 = 1$, corresponds to the single-photon recoil limit. See Table 2 for other quantitative details.

Next, we consider the other case of experimental interest, the Maxwellian thermal beam having a flux distribution

$$W_M(U) = 2U^3V^{-4} \exp(-U^2/V^2), \quad (77)$$

where V is now a thermal velocity. For a thermal flux, the distribution width v , still defined by Eq. (68c), is not small,

$$v = \sqrt{64/9\pi - 2} \approx 0.513. \quad (78)$$

On the other hand, since $v \lesssim 1$, we expect that the order of magnitude of the density's peak amplitude, the spot size (or spatial resolution) of the lens, and the focal position should be the same. In analogy with the analysis above, we consider the atomic density at a distance L from the SW lens, where $L = Vt_0$ is now defined by the free evolution time t_0 for an atom with thermal velocity V . (The average thermal flux velocity U_0 is given by $3\sqrt{\pi}V/4 \approx 1.33V$.)

We can now use the thermal flux distribution (77) in Eq. (70) to calculate the various, exact lens parameters. To find the focus for this distribution, instead of monitoring the peak atomic density $\bar{\rho}(0, t_0)$, we monitor the thermally-averaged density contrast $\bar{c}(t_0) = \bar{\rho}(0, t_0)/\bar{\rho}(\pi, t_0)$ from Eq (44). An example of $\bar{c}(t_0)$ for $\theta_0 = 23.0$ is shown in Fig. 9. The focal plane position is defined by the time when $\bar{c}(t_0)$ is largest, $t_0 = t_f$ ($L = Vt_f$). The atomic density at t_f , $\bar{\rho}(x, t_f)$, for this pulse area is also shown in Fig. 9. Several lens parameters as functions of θ_0 are shown in Fig. 10, including

the focal time t_f , the contrast at the focal plane $c(t_f)$, and the spot size w .

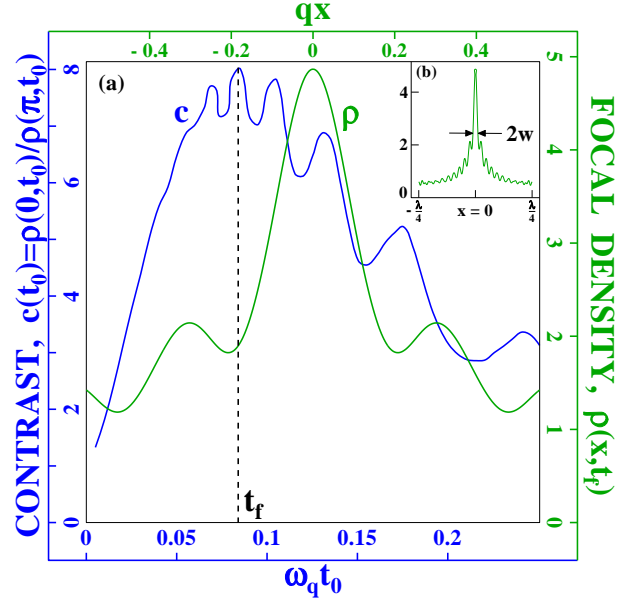


FIG. 9. Thermal longitudinal beam focusing. (a) Time evolution of the atomic density contrast, $c(t_0) = \bar{\rho}(0, t_0)/\bar{\rho}(\pi, t_0)$, and the density profile at the focal plane, $\bar{\rho}(x, t_f)$. (b) Atomic density profile at the focus, $\bar{\rho}(x, t_f)$, plotted in the range $-\lambda/4 \leq x \leq \lambda/4$. The pulse area for these curves, $\theta_0 = 23.0$, is needed to produce a spot size of $w = 6.5 \text{ nm}$ in Na using a thermal beam.

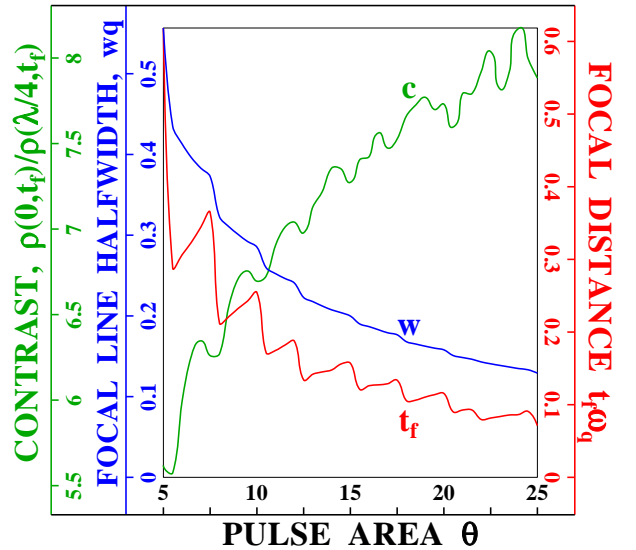


FIG. 10. Thermal longitudinal beam focusing. Exact pulse area dependence of the focusing parameters: Focal density contrast $c(t_f) = \bar{\rho}(0, t_f)/\bar{\rho}(\pi, t_f)$, focal distance t_f , and spot size w (HWHM of the density profile at the focal plane).

B. Transverse velocity distributions: Angular beam divergence/Trap velocity distributions

Transverse velocity distributions put an additional constraint on the thin SW lens performance and have been a limiting factor in Fresnel atom optics and interferometry. For an atom beam, the angular divergence is equivalent to the transverse velocity distribution of atoms in a cold trap, again allowing a time domain treatment. The transverse and longitudinal beam velocities are generally related linearly by the angle in the paraxial limit. This is the case both for atomic beams collimated by apertures and for beams that are laser-cooled in the transverse direction. Given that we have already discussed chromatic aberration in detail, here we present comparative focal parameters and densities which include either transverse effects alone or simultaneous longitudinal and transverse velocity effects. Only the narrow longitudinal velocity atom beam will be considered in detail since this type of beam leads to a better focus.

We will look at two cases. For both cases the Fourier method suggests a straightforward interpretation of the effects of a transverse velocity distribution in terms of an inhomogeneous decay of the density spatial harmonics. First, we treat the case where the beam is monochromatic as in Sec. II and the transverse velocity distribution is either a uniform or one-dimensional Maxwellian (thermal) distribution of transverse velocities. The uniform distribution might apply to an atomic beam collimated by a slit or a pair of slits while the thermal distribution might apply to a laser-cooled beam or to atoms released from a laser-cooled trap. The resulting focal parameters and densities for the slit-collimated and laser-cooled atoms are similar qualitatively. Then, we consider a more general beam case where the transverse velocity and longitudinal flux distributions are *decoupled*, but the longitudinal velocity dependence of the time *couples* the transverse integration to the longitudinal. This applies to atomic beams that are laser cooled before interacting with the SW lens. The theoretical treatment of each of these cases is facilitated by the Fourier method.

Our first case is the monovelocity longitudinal beam ($v \rightarrow 0$) with a transverse velocity distribution $P(U_x)$. To unify the longitudinal and transverse results, we start with Eq. (70) and take $W(U) = \delta(U - U_0)$. This is equivalent to starting from Eq. (21a) or (21b) and taking $U = U_0$, $t = t_0$, and $\theta = \theta_0$. Assuming we are describing the atomic beam rather than the trap, the atoms are again detected, deposited, or used for lithography at $L = U_0 t_0$. The inclusion of an initial transverse velocity U_x during the atom-field interaction will lead to a Doppler shift of the field frequency. (Note that the dimensionless transverse velocity scale that is consistent with the dimensionless variables (20) is the single-photon recoil velocity, $V_k = \hbar q/2M$.) We rigorously account for the Doppler shift by taking $x \rightarrow x + U_x t$ and averaging the density over $P(U_x)$,

$$\rho(x, t_0) = \sum_{n=-\infty}^{\infty} e^{inx} J_n[\theta_0 \sin(nt_0)] \int dU_x P(U_x) e^{inU_x t_0}. \quad (79)$$

The assumption is that the initial transverse density matrix is diagonal in momentum space and can be described by a normalized velocity distribution $P(U_x)$. In terms of the longitudinal velocity U_0 of the beam, the transverse velocity can be written as $U_x = U_0 \varphi$, where φ is the propagation angle with respect to the z -axis.

The two transverse distributions of interest, the uniform distribution $P_1(U_x)$ and Maxwellian distribution $P_2(U_x)$, take the following form for $V_x \ll U_0$:

$$1. P_1(U_x) = (2V_x)^{-1} \text{ for } U_x \in [-V_x, V_x], \quad (80a)$$

$$2. P_2(U_x) = (\sqrt{\pi}V_x)^{-1} \exp[-(U_x/V_x)^2]. \quad (80b)$$

Each can be written as a distribution over beam angles φ , if desired, by defining the divergence angle $\varphi_d \equiv V_x/U_0$. The first distribution might be formed when a thermal transverse distribution, peaked at $U_x = 0$ ($\varphi = 0$) with velocity width much greater than V_k , is collimated by a pair of slits which select a small range of propagation angles up to φ_d . This beam has a *rms* transverse velocity spread of $V_1 = V_x/\sqrt{3}$. The second distribution might be formed by transverse laser cooling, with or without previous slit collimation, and has a *rms* velocity width of $V_2 = V_x/\sqrt{2}$. (Technically, the laser cooling process can create a non-diagonal density matrix with transverse momentum state coherences that are not accounted for here but can be incorporated into a more general Fourier result. We assume the distribution is narrow and diagonal.)

Fortuitously, both distributions again give closed-form Fourier coefficients for the density. Inserting Eqs. (80) into Eq. (79), one finds

$$1. \rho(x, t_0) = \sum_{n=-\infty}^{\infty} e^{inx} \frac{\sin[nV_x t_0]}{nV_x t_0} \times J_n[\theta_0 \sin(nt_0)]; \quad (81a)$$

$$2. \rho(x, t_0) = \sum_{n=-\infty}^{\infty} \exp[inx - (nV_x t_0/2)^2] \times J_n[\theta_0 \sin(nt_0)]. \quad (81b)$$

The interpretation is the same as for an atomic free induction decay experiment [13]. The harmonics of the total density undergo an inhomogeneous decay as each velocity class U_x evolves with its own Doppler-shifted frequency. The P_1 result was recently explained in detail as it is isomorphic to the evolution of a model, one-dimensional BEC or a degenerate Fermi gas after interacting with a SW pulse [29]. A similar expression to the P_2 result was used recently to explain the decay of periodic echoes [13] and the decay of a quasiperiodic atomic focusing and Talbot scheme [27]. For both distributions

the harmonic decay functions of Eqs. (81) depend on $nV_x\theta_0^{-1}$ near the focus, $t_0 \sim \theta_0^{-1}$. For $V_x \lesssim 1$ only harmonics greater than $n_{\max} \simeq \theta_0$ undergo significant damping, so it appears that the transverse velocity width can be up to the order of the recoil velocity to avoid a significant decay of the high-order Fourier components necessary for a highly-peaked focus. However, the restriction $V_x \lesssim 1$ may be sufficient but not necessary. We have found in the previous sections that the lens parameters scale with θ_0 , and, therefore, in Sec. V we show that the restriction on V_x is somewhat relaxed.

The focal distance t_f , defined as the first maximum of Eq. (81a) or (81b), moves closer to the lens for $V_x > 0$ when compared to the focal distance for $V_x = 0$. This makes sense since the transverse distribution causes a decay in the modulated density in time. However, this shift of the focal distance is secondary in importance to the changes in the peak density at the focus and the spot size. Moreover, as θ_0 increases, the focal distance including the transverse velocity spread converges rapidly to the ideal value near $t_0 \simeq \theta_0^{-1}$. We have calculated the peak density and spot size for selected values of V_x and compared them to the ideal case. In Fig. 11 the peak focal density, $\rho(0, t_f)$, and spot size w are plotted versus θ_0 for $V_x = 0$ (ideal), $V_1 = V_2 = 1$ (recoil limit), and $V_1 = V_2 = 2$ (twice the recoil limit). For each of the five curves, the exact, different focal time at each value of θ_0 is used to calculate the parameters. For the same *rms* velocity spread, the P_2 distribution gives a narrower, more peaked density spot than the P_1 distribution. It is significant that the percentage error in the peak density and spot size is decreasing as θ_0 increases. This result is expected since inhomogeneous decay is less pronounced at earlier times, $t_0 \sim \theta_0^{-1}$.

To treat the full problem of focusing an atomic beam with velocity distributions more generally, we must account for the angular relation between the longitudinal and transverse velocities. The atomic velocity in a beam, $\mathbf{U} = U\hat{z} + U_x\hat{x}$, can be written $\mathbf{U} \simeq |\mathbf{U}|\hat{z} + |\mathbf{U}|\varphi\hat{x}$ for small angles φ , where $|\mathbf{U}| \simeq U$ to lowest order in φ in the paraxial approximation. Since atomic beams are inherently formed by a process which truncates either the divergence angle or the transverse velocity distribution, it is not a simple matter to describe them theoretically. However, if the beam is localized around some large longitudinal speed and then laser cooled in the transverse direction before the SW lens, the longitudinal and transverse distributions are effectively independent. We can model the total (normalized) flux probability $W(\mathbf{U})d\mathbf{U}$ as a product of the two independent distributions, $W_{LM}(U)P_2(U_x)dUdU_x$, using the local Maxwellian longitudinal flux distribution $W_{LM}(U)$, Eq. (76a), and thermal transverse velocity distribution $P_2(U_x)$, Eq. (80b).

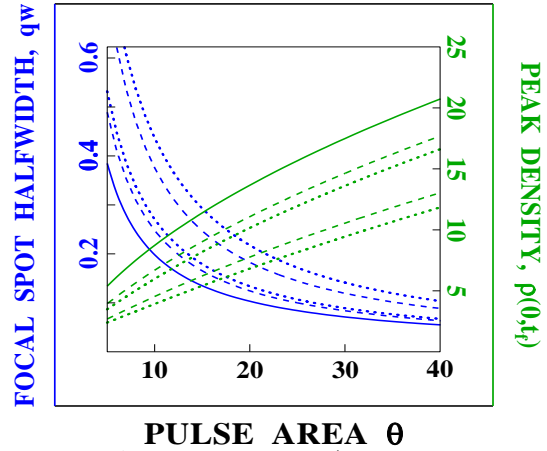


FIG. 11. Angular divergence (transverse velocity distribution) in atom focusing, neglecting chromatic aberration. Exact pulse area dependence of the lens parameters: Peak focal density $\rho(0, t_f)$ and spot size w (HWHM of the density profile at the focal plane). The solid curves are for the ideal atom beam (with no angular divergence), the dotted curves are for the uniform transverse distribution (P_1), and the dashed curves are for the Maxwellian distribution (P_2). The middle pairs of curves, closest to the ideal case, are for $V_1 = V_2 = 1$, the *rms* single-photon recoil limit. The outer pairs are for $V_1 = V_2 = 2$, twice the recoil limit.

Since the time of flight, $t = L/U$, to the detection plane, $L = U_0 t_0$, depends on the longitudinal velocity, the Doppler phase $e^{inU_x t_0 U_0/U}$ does as well. Inserting the integration of the Doppler phase over the distribution $P_2(U_x)$ into Eq. (70), we find the velocity-averaged density to be

$$\bar{\rho}(x, t_0) = \sum_{n=-\infty}^{\infty} e^{inx} \int_0^{\infty} dU W(U) \exp[-(nV_x t_0 U_0/2U)^2] \times \{J_n[(\theta_0 U_0/U) \sin(n t_0 U_0/U)]\}. \quad (82a)$$

The Fourier component of the density now has an additional Gaussian multiplier to integrate over longitudinal velocities. If the longitudinal width v is small but non-negligible and we want $V_x \lesssim 1$ (laser cooling to the recoil limit), the argument of the Gaussian is on the order of the argument of the sine function. As a result, we cannot neglect the Gaussian decay in the integral by assuming $W(U)$ is sharply peaked around U_0 and thus evaluating it at $U = U_0$ ($v \rightarrow 0$ limit). In Sec. V we treat two examples of experimental interest with this expression, an atomic beam which is laser-cooled to the transverse recoil limit, both with and without a longitudinal flux width v . This is shown in Fig. 8 along with the ideal and purely longitudinally-broadened cases.

V. DISCUSSION

In this article we have developed a theory of atom focusing by standing wave light fields in the thin lens regime. We have shown that the exact analytical expressions for the Fourier components of the atomic density, recently used in the theory of atom interferometry, are useful for numerical calculations of the focusing effect and all its relevant lens parameters, including the effects of chromatic aberration and angular divergence. We call the Fourier technique Method 1.

Thin lens focusing becomes especially effective for a large field area θ . When $\sqrt{\theta} \gg 1$ for the monovelocity case, using the Fresnel-Kirchhoff diffraction integral, we can consider only the first anharmonic term of the phase shift created by the SW light field when expanding around the potential wells at $x' = 2\pi m$. This procedure, labeled Method 2, leads to a manageable expression (30) for the atomic density distribution which can be used to evaluate the focal parameters by numerical integration.

Within a small vicinity of the focal time, Eq. (30) simplifies further to the asymptotic density profile (36). This is Method 3. The analytical correction to the focal time and analytical expressions for the peak focal density, spot size, and depth of focus as functions of the pulse area θ follow from this result. The last three lens parameters scale as $\theta^{1/2}$, $\theta^{-3/4}$, and $\theta^{-3/2}$ respectively, while the focal time scales as $\theta^{-1} \left(1 + 1.27\theta^{-1/2}\right)$ [see Eqs. (39), (40), (41), and (42)]. From Fig. 3 one sees that in the range $0 < \theta < 40$, the accuracy of the Method 3 asymptotic expressions for the peak focal density, focal time, and spot size can be as small as 17%, 1.9% and 18% respectively. The asymptotic parameters obtained by Method 2 using Eqs. (30) are generally more precise, giving accuracies for the same parameters as small as 5.8%, 0.24% and 4%, respectively.

The accuracy of the asymptotic result for the focal time t_f is an order of magnitude better than for other focusing parameters. Evidently, this is a consequence of the fact that a finite value for the focal time, $t \sim \theta^{-1}$, comes out of the harmonic approximation for the lens potential. The first anharmonic term then leads to a relative correction of the order of $\theta^{-1/2}$ [see Eq. (39)], and higher-order anharmonic corrections (not included in our consideration) should have relative weights θ^{-1} and larger inverse powers of θ . As for the other parameters, which can be derived only by including the first anharmonic term, the next order corrections should have a larger relative weight of $\theta^{-1/2}$.

For example, the constant offsets of the asymptotic peak densities from the exact result in Fig. 3 can be explained as follows. A correction to the asymptotic wave function at $x = 0$ [Eq. (31)] of relative weight $\theta^{-1/2}$ would result from including the next order spherical aberration, the x'^6 term in the expansion of $\cos(x')$ in Eq. (28a). When the wave function is squared to form the density, this relative correction of weight $\theta^{-1/2}$ multiplies

the lowest-order peak density that grows as $\theta^{1/2}$ to give a constant term, which is automatically accounted for by the exact Fourier method. Hence, the constant offset of the asymptotic peak density is not included in our asymptotic expressions.

In this article we have also analyzed a new type of atom focusing which arises when the SW field is resonant with the atomic transition. The density profiles and focal parameters for the resonant lens are shown in Figs. 4 and 5, respectively. To gain insight into the different interactions that can lead to focusing, we can consider the far-detuned and resonant cases from a more general point of view than that taken in Secs. II and III, still assuming that the field envelope is short enough to neglect spontaneous emission during the pulse. When an atom interacts with a pulsed light field, the states of the system can be decomposed into a set of semiclassical dressed states of the atom plus field. If the atom-field interaction is adiabatic or the pulse turns on instantaneously, these dressed states are instantaneous eigenstates of the total Hamiltonian and therefore undergo a phase modulation. When the light field modes have a modulated intensity, the dressed state energies and, therefore, phase evolutions are also spatially modulated. Focusing can occur near the intensity extrema, which correspond to spatial minima of the dressed state energies. If initially the bare atom was in a pure state such as the ground state $|g\rangle$, the atomic wave function after the interaction is generally a coherent admixture of the two dressed states, which have an energy separation that is spatially modulated. Therefore, an interference term in squaring the bare state amplitudes can lead to a Rabi-like oscillation of the total density and its properties. This Rabi-like oscillation can be seen in Eq. (65a) and Fig. 5 for a resonant SW field. Nonadiabatic, detuned atom-field couplings can lead to a similar effect. The evolution of the pure and dressed states in this regime has been considered previously without center-of-mass spatial effects [43]. For the far detuned standing wave ($|\Delta| \gg |\chi|$) or an adiabatic turn-on of the field, the ground state evolves into only one of the dressed states while the other dressed state has a negligible amplitude. As a result, one does not observe any interference or field dependent oscillation in this case.

Up to this point in the discussion, we have reviewed the ideal situation of the ideal atomic beam having no angular divergence and no longitudinal velocity distribution. Our calculations in the thin lens regime have shown that focusing results in a relatively large peak focal density. For the most part, this result is in contrast to previous experiments carried out in the thick lens regime, where it proved difficult to achieve such large density peaks. The exceptions are certain experiments in Na at $\lambda = 589 \text{ nm}$ on the $3S_{1/2}, F = 2 \rightarrow 3P_{3/2}, F' = 3$ transition [6,7]. In these thick lens experiments for a thermal beam having thermal velocity $V \simeq 8.6 \times 10^4 \text{ cm/s}$, the spot size resolution and contrast were $w = 10 \text{ nm}$, $c(t_f) = 10$ [6] and $w = 6.5 \text{ nm}$, $c(t_f) = 6$ [7], respectively. As an exercise,

we can compare that experimental data using a thermal beam and thick SW lens with our results using a ideal atomic beam and thin lens. From Fig. 3 or an exact calculation, a pulse area of $\theta \simeq 14.86$ (9.37) is needed for a resolution of $qw = 0.139$ ($qw = 0.139$), or $w = 6.5$ nm (10 nm) in sodium. If we set the beam velocity U equal to 8.6×10^4 cm/s, then focusing for $\theta \simeq 14.86$ occurs at a distance $L_f = Ut_f = 127$ μ m. The atomic density profile at this distance is shown with the thin solid line in Fig. 8. The contrast at the focus, defined by Eq. (44) as the ratio of focal atomic densities at $qx = 0$ and $qx = \pi$ (not shown in Fig. 8), is $c(t_f) = 27.2$.

We can determine the standing wave power needed to achieve a pulse area of $\theta = 14.86$ for the two-level system. This system can be realized in Na using optical pumping to the ground state sublevel having magnetic quantum number $m_F = \pm 2$. A circularly polarized standing wave drives only the $3S_{1/2}$, $F = 2$, $m_F = \pm 2 \rightarrow 3P_{3/2}$, $F' = 3$, $m_{F'} = \pm 3$ transition which has the dipole moment matrix element $|\mu| = 6.37 \times 10^{-18}$ esu \cdot cm. To achieve the intensity necessary for atomic focusing, the SW field must be formed by focused laser beams. In the experiments of Refs. [6,7], the fields have been focused to a circular spot having radius $\sigma_z \simeq 29$ μ m [44]. For experiments in the thin lens regime, it is sufficient to focus the field only in the z -direction, along which the atomic beam propagates. We assume that the laser field intensity has a Gaussian profile in the (y, z) plane,

$$|E(y, z)|^2 = |E|^2 \exp(-2y^2/\sigma_y^2 - 2z^2/\sigma_z^2), \quad (83)$$

where σ_z and σ_y are field radii along the z - and y -axes, respectively (i.e., the directions perpendicular to the laser beam propagation along the x axis). For homogeneous atomic focusing into a set of lines, one should choose σ_y to be larger than the atomic beam radius. From the data in Refs. [6,7], σ_y should be as large as 0.5 cm. The general field mode (83) can be created using cylindrical optical lenses. The far-detuned pulse area θ (10) can be re-expressed through the constituent traveling wave field powers of Eqs. (1) and (83), $P = c|E|^2 \sigma_z \sigma_y / 16$, as $\theta = -\sqrt{\pi} 2^{7/2} |\mu|^2 P / (\hbar^2 c \sigma_y \Delta U)$. For further estimates we assume that $\sigma_z = 29$ μ m, $\sigma_y = 0.5$ cm, and $\Delta = -2\pi \cdot (1.71$ GHz). Then, for a field area of $\theta = 14.86$, the required laser power is $P = 1.89$ mW. Even this power level is four times less than the power used in the experiment of Ref. [7]. To compare directly to the circular focus of the field in Ref. [7], we must take $\sigma_y = 29$ μ m, giving us a required power of $P = 11.0$ μ W. These relatively low power levels are sufficient for our consideration of thin lens focusing.

We can now discuss the influence of chromatic aberration assuming no angular divergence. A longitudinal velocity distribution in the atomic beam leads to a degradation of the focus. But even for the thermal beam, the normalized distribution width v is still less than 1 [see Eq. (78)], and we have shown that the order of magnitude of the focusing parameters is the same as for the

ideal beam ($v = 0$). For narrow flux distributions, $v \ll 1$, the lowest-order corrections to the atom density behave as v^2 [see Eqs. (73)] if $\theta \gtrsim 1$. This is a simple consequence of the fact that terms linear in the deviation from the average atomic flux vanish after averaging over velocities for any symmetric, or asymmetric, distribution. In particular, this principle applies to the analytical Fourier components of the density multiplied by the narrow, local Maxwellian flux distribution $W_{IM}(U)$, Eq. (70), for small v .

In Fig. 7 we show the exact (using $W_{IM}(U)$) and approximate reductions of the density at the ideal beam focal time, $\bar{\rho}(0, t_{0,f})/\rho(0, t_{0,f})$ [42], as functions of v for two values of θ_0 , 14.86 and 9.37. Again, these choices for θ_0 are the pulse areas required to achieve $w_0 = 6.5$ and 10 nm spot sizes [6,7], respectively, using ideal sodium beams. The quadratic dependence, consistent with Eqs. (74c), is evident for small v , but the exact density peak actually reduces more slowly (linearly) at larger values of v where the small v approximation breaks down. At this point the expansions of the Bessel functions of Eq. (70) near $t_{0,f} \approx \theta_0^{-1}$ in terms of u are invalid since $n_{\max} \langle |u| \rangle \gtrsim 1$, or equivalently $v \sim \theta_0^{-1}$: a term proportional to $|u|$ would appear in an expansion around the average velocity. We take this as evidence that near this value of v for a fixed θ_0 , the focal properties go from being dominated by spherical aberration to a regime where a more complicated combination of spherical and chromatic aberrations is important.

To test this idea, we have also examined the dependence of the spot size increase, w/w_0 , on v for $\theta_0 = 14.86$ and 9.37 using the exact density for $W_{IM}(U)$. In Fig. 7 the spot size's quadratic dependence for small v turns into a linear dependence near the same value of v that the peak density reduction deviates from the approximate theory. We see that the chromatic aberration has a smaller effect on the spot size than on the peak density. Note that from a ray tracing argument for far-field focusing through an effective parabolic lens aperture of full width $\sim \lambda/2$, a strong, θ -independent, linear dependence of $w \propto \pi v$ (or equivalently $\langle |u| \rangle$) would be expected for a focus dominated by chromatic aberration in the absence of spherical aberration [19]. However, this is not the case for the SW field lens, where spherical aberration determines the limiting resolution up to large values of θ_0 . Thus, the chromatic aberration we find is less severe and depends strongly on θ_0 . We have not explored this θ_0 dependence further. However, from Fig. 7 we deduce that if we fix v (and by implication the atomic beam properties), a threshold pulse area, $\theta_{th} \sim v^{-1}$, must exist for each v to mark the breakdown of the small v expansion. For $\theta_0 \gtrsim \theta_{th}$ the effects of chromatic aberration should be calculated exactly.

To further demonstrate the small v results for a narrow longitudinal distribution, we can define α to be the percentage reduction of the peak focal density as a function of θ_0 and v . The flux distribution width for a given

θ_0 and α is therefore $v = \sqrt{\alpha\rho(0, t_{0,f})/\rho_1(0, t_{0,f})}$ from Eq. (74c). From Fig. 6 or 7 for $\theta_0 = 14.86$, to limit the peak density reduction to $\alpha = 10\%$, we can estimate that a normalized flux width of $v \simeq 0.086$ would be needed. (For the local Maxwellian distribution, $W_{LM}(U)$, a flux width of $v \simeq 0.091$ is found to be sufficient by an exact calculation with Eq. (70).) Using $v \simeq 0.086$ to calculate the other parameters approximately from Eqs. (74b) and (74e), the percentage corrections to the focal distance and spot size are even less than α , 3.9% and 1.3%, respectively. A longitudinal width, $v \simeq 0.086$, is typical of the supersonic beams produced by seeding an inert (noble) gas supersonic expansion with sodium [45]. While the mean longitudinal velocity of a beam produced recently from a BEC of sodium atoms by Bragg scattering [14] was only $2\hbar k/M$, or 6 cm/s , the *rms* longitudinal and transverse velocity widths were only approximately $0.16\hbar k/M$ and $0.30\hbar k/M$, respectively, giving $v \simeq 0.11$ and justifying the paraxial approximation. In these experiments, mean longitudinal velocities up to $11.9\hbar k/M$, or 35 cm/s , with similar widths were also achieved using higher-order Bragg scattering, implying $v \ll 0.1$. Since experiments producing atomic beams of this type are in their infancy, we expect that achieving relative velocity widths of $v \ll 0.1$ will shortly become routine.

In Fig. 8 the atomic distribution at the focus $\bar{\rho}(x, t_f)$ (dotted line), as calculated exactly using $W_{LM}(U)$ in Eq. (70) for $\theta_0 = 14.86$ and our extreme case from Fig. 7 of $v \simeq 0.194$ ($V/\tilde{U}_0 = 0.2$), is compared to the ideal case (thin solid line). While the reduction of the peak density from 11.4 to 7.81 is a significant 31% on a scale where ~ 0.5 is the background at the focus, the half-width defining the spot size is broadened by only 5% (or 0.33 nm in sodium), and the coherent oscillations of the density along x are still prevalent. This suggests that even for $v \approx 0.2$ and a focal peak reduced by chromatic aberration, a high resolution, large contrast focus is possible with the thin SW lens. In addition, using the flux distribution $W_{LM}(u)$ with $v = 0.194$, we have also calculated that the field area, $\theta_0 = 15.7$, is required to restore a spot size of $qw = 0.139$, or 6.5 nm in sodium. This corresponds to the laser power, $P = 2.0\text{ mW}$, for $\sigma_z = 29\text{ }\mu\text{m}$, $\sigma_y = 0.5\text{ cm}$, and $\Delta = -2\pi \cdot (1.71\text{ GHz})$.

We have also considered the focusing of a thermal atomic beam with flux $W_M(U)$. The results of the calculations are graphed in Figs. 9 and 10. For this part of the paper only, we changed the definition of the focal distance to be one where the contrast (44), and not the density, is optimized. The contrast, $c(t_0) = \bar{\rho}(0, t_0)/\bar{\rho}(\pi, t_0)$, for $\theta_0 = 23.0$ at a distance L from the SW field ($t_0 = L/V$) is shown in Fig. 9. We see that $c(t_0)$ contains three local maxima of approximately equal weight near the focus. They arise as a result of the time-oscillations of the flux-averaged, background atom density near $t_0 = t_f$, $\bar{\rho}(\pi, t_0)$. These contrast maxima "compete" with one another in some sense as different values of the pulse area correspond to different velocity classes and there-

fore different focal distances. This effect results in the discontinuities in the pulse area dependences of the lens parameters seen in Fig. 10.

For the longitudinal thermal beam and $\theta_0 = 23.0$, the focal contrast is equal to $c(t_f) = 8.03$ while the spot size or spatial resolution is again $qw = 0.139$. For the same experimental parameters as above, $\sigma_z = 29\text{ }\mu\text{m}$, $\sigma_y = 0.5\text{ cm}$, and $\Delta = -2\pi \cdot (1.71\text{ GHz})$, a laser field power of $P = 2.9\text{ mW}$ is needed to produce a pulse area of $\theta_0 = 23.0$.

Finally, the atomic beam angular divergence has a crucial impact on the focus, independent of the chromatic aberration. For a beam with no chromatic aberration, $U = U_0$, if atoms move at an angle φ with respect to the z -axis, the density profile displaces a distance $\delta x \sim U_0\varphi t_f \simeq U_x t_f$ along the x axis. This displacement should ideally be much smaller than the fundamental spot size w that accounts for spherical aberration. We can use the previously generated, exact spot sizes and focal times for each θ_0 to estimate the maximum allowed *rms* transverse velocity from this argument, $V_{rms}^{(f)} \approx w/t_f$. This corresponds to an angular divergence $\varphi_f = V_{rms}^{(f)}/U_0 \approx w/(t_f U_0)$. We expect that allowing V_{rms} to be $V_{rms}^{(f)}$ will at most double the spot size.

Alternatively, from Eqs. (39) and (41) for dimensionless t_f and w , the asymptotic restriction on the angular divergence, $\varphi \lesssim \varphi_f$, is

$$\varphi_f \sim 0.744 \frac{\hbar q}{2MU_0} \theta_0^{1/4} (1 - 1.27\theta_0^{-1/2}) \sim 0.744 \frac{V_k}{U_0} \theta_0^{1/4}. \quad (84)$$

It is interesting to note that the asymptotic focusing restriction is $\sim \theta^{1/4}$ times less severe than the recoil limit,

$$\varphi \ll \varphi_T \sim \frac{\hbar q}{2MU_0} \equiv \frac{\lambda_{dB}}{\lambda}, \quad (85)$$

which is the condition required to observe atom interference in the single interaction region geometry (for example, the atomic Talbot effect [26,25,33,34]). Condition (85) arises from the requirement that atoms moving at an angle φ not be displaced more than $\lambda/2$ at the Talbot distance $L_T \sim \lambda^2/2\lambda_{dB}$. Even though effective focusing requires the displacement to be $\theta^{3/4}$ times smaller asymptotically (since $qw \propto \theta^{-3/4}$), this displacement occurs at a distance that is θ -times shorter than the Talbot distance (since $L_f = U_0 t_f \sim L_T/\theta_0$).

This argument is consistent with Eqs. (81) and Fig. 11. This figure suggests that small spot sizes with sharp density peaks can be achieved for laser powers in the microwatts to milliwatts range even for transverse distribution widths larger than the recoil limit. (In Fig. 11, note that $qw = 0.3$ corresponds to a 14 nm spot size in sodium.) For example, taking $\theta_0 = 40$ and remembering that the slit-collimated beam has a *rms* transverse velocity V_1 ($V_x\sqrt{3}$) in units of V_k , the exact spot size

for $V_1 = 0$ is $qw = 0.0577$ from Eq. (81a). Now, assuming the divergence is the maximum allowed, we set $V_1 = w/t_f = 1.883$ for $\theta_0 = 40$ and find that the spot size is broadened to 0.100 (4.69 nm in sodium), or 73%. The spot size has less than doubled for a transverse width almost twice the recoil limit. Similarly, the asymptotic predictions for $\theta_0 = 40$ give an increase from a spot size of $qw = 0.0468$ (not 0.0577) for $V_1 = 0$ to a spot size of 0.0826 for $V_1 = U_0\varphi_f = 1.495$ from Eq. (84) in Eq. (81a), a 76% increase. The broadening is even less severe for Maxwellian transverse distributions.

We now take a case of experimental interest to demonstrate the combined effects of transverse and longitudinal broadening on the focal density. The pulse area, $\theta_0 = 14.86$, is used again. We show results for the P_2 (Maxwellian) transverse distribution, Eq. (80b), since laser cooling has been shown to improve the focus in thick lens experiments [5–7]. In Fig. (8) we plot the density at the focus $\rho(x, t_f)$ (dashed line) from Eq. (81b) for a monochromatic beam ($v \rightarrow 0$) cooled to the *rms* single-photon recoil limit, $V_2 = 1$ ($V_x = \sqrt{2}$). In addition, we show the atomic focal density (lower solid line) from Eq. (82a) for $\theta_0 = 14.86$, $v = 0.194$ ($V/\tilde{U}_0 = 0.2$ in $W_{IM}(U)$), and $V_2 = 1$. The latter curve combines the attributes of the other curves in this figure to provide a real picture of the focus. The following table summarizes the results for Fig. 8:

Table 2. Focusing of an atomic beam for $\theta_0 = 14.86$. A velocity-averaged spot of $qw = 0.190$ corresponds to 8.91 nm in sodium, for which $V_k \simeq 2.95$ cm/s and $\omega_q \simeq 6.29 \times 10^6$ rad/s.

Atomic Beam	v	$\frac{V_x}{V_k}$	$\omega_q t_f$	$\rho(0, t_f)$	qw	$\rho(\pi, t_f)$	$c(t_f)$
Ideal	0	0	.0930	11.4	.139	.420	27.2
Chromatic Aberration	.194	0	.0856	8.06	.146	.438	18.4
Angular Divergence	0	$\sqrt{2}$.0893	9.06	.169	.430	21.1
Combined	.194	$\sqrt{2}$.0814	6.64	.190	.450	14.8

Our work suggests emphatically that the thin SW lens can focus atoms effectively if the angular divergence is cooled near the recoil limit, even in the presence of strong chromatic aberration. This makes physical sense if one considers that the longitudinal velocity average over slightly different focal regions for each velocity subclass is a slowly-varying integral over the Fourier *amplitudes* when compared to the more sensitive transverse velocity integral, an average over the Doppler *phases*. Atomic beams of the type considered throughout this article can be made in the laboratory with current technology.

In addition to the experimental possibilities for standard atomic beams that limit angular divergence by slit collimation or transverse laser cooling, recent experiments that use higher-order Bragg diffraction of a BEC to form atomic beams with transverse and longitudinal

rms velocities smaller than the recoil velocity [14] offer a promising avenue to observe and characterize thin lens focusing effects. We would even argue that focal patterns nearly identical to those described in this paper have already been achieved but not recognized in recent condensate experiments on the so-called momentum space Talbot effect [46]. In these experiments a cloud of cold atoms from a condensate interacts with two off-resonant SW pulses, separated by a variable time delay. The detection scheme is insensitive to Fresnel effects as the researchers image the far-field diffraction pattern and therefore the atomic momentum distribution. However, the accurate fit of the data in that experiment to our Raman-Nath theory suggests that the thin lens focusing effect is occurring after the first pulse along the SW grating direction. A detection scheme sensitive to the Fresnel density pattern may be necessary to image the focusing atoms in the cloud.

ACKNOWLEDGMENTS

J.L.C. is indebted to Prof. Tycho Sleator and the NYU Physics Department for providing him with the Visiting Scholar appointment during which this work was completed. This work is supported by the National Science Foundation under Grants No. PHY-9414020 and PHY-9800981, by the U.S. Army Research Office under Grant No. DAAG55-97-0113 and AASERT No. DAAH04-96-0160, and by the University of Michigan Rackham predoctoral fellowship.

-
- [1] M. Prentiss, G. Timp, N. Bigelow, R.E. Behringer and J.E. Cunningham, Appl. Phys. Lett. **60**, 1027, (1992).
 - [2] T. Sleator, T. Pfau, V. Balykin and J. Mlynek, Appl. Phys. B **54**, 375, (1992).
 - [3] G. Timp, R.E. Behringer, D.M. Tennant, J.E. Cunningham, M. Prentiss, K. Berggren, Phys. Rev. Lett. **69**, 1636 (1992).
 - [4] J.J. McClelland, R.E. Scholten, E.C. Palm, and R.J. Celotta, Science **262**, 877 (1993)
 - [5] R.E. Behringer, V. Natarajan, G. Timp, Appl. Phys. Lett. **68**, 1034 (1996).
 - [6] V. Natarajan, R. E. Behringer, and G. Timp, Phys. Rev. A **53**, 4381 (1996).
 - [7] R.E. Behringer, V. Natarajan, G. Timp, and D.M. Tennant, J. Vac. Sci. Technol. B **14**, 4072 (1996).
 - [8] R.J. Celotta, R. Gupta, R. E. Scholten, J.J. McClelland, J. Appl. Phys. **79**, 6079 (1996).
 - [9] U. Drodofsky, M. Drewsen, T. Pfau, S. Novak and J. Mlynek, Microelec. Eng. **30**, 383 (1996).
 - [10] U. Drodofsky, J. Stuhler, B. Brezger, Th. Schulze, M. Drewsen, T. Pfau and J. Mlynek, Microelec. Eng. **35**, 285 (1997).

- [11] J.J. McClelland, "Nanofabrication via Atom Optics," NIST Electronic Physics Group, Preprint, to appear in *Handbook of Nanostructured Materials and Nanotechnology*, ed. by H. S. Nalwa, to be published by Academic Press.
- [12] K.K. Berggren, A. Bard, J.L. Wilbur, J.D. Gillaspay, A.G. Heig, J.J. McClelland, S.L. Rolston, W.D. Phillips, M. Prentiss, and G.M. Whitesides, *Science* **269**, 1255, (1995); S. Nowak, T. Pfau and J. Mlynek, *Appl. Phys. B* **63**, 203 (1996); K.S. Johnson, K.K. Berggren, A. Black, C. Black, A.P. Chu, N. Dekker, D. Ralph, J.H. Thywissen, R. Younkin, M. Prentiss, M.Tinkham, and G. Whitesides, *Appl. Phys. Lett.* **69**, 2773 (1996)
- [13] S.B. Cahn, A. Kumarakrishnan, U. Shim, T. Sleator, P.R. Berman and B. Dubetsky, *Phys. Rev. Lett.* **79**, 784 (1997).
- [14] M. Kozuma, L. Deng, E.W. Hagley, J. Wen, K. Helmerston, S.L. Rolston, and W.D. Phillips, *Phys. Rev. Lett.* **82**, 871 (1999).
- [15] K. Berggren, M. Prentiss, G. Timp, R.E. Behringer, J. Opt. Soc. Am. **B11**, 1166 (1994).
- [16] R. Gupta, J. J. McClelland, P. Marte, R.J. Celotta, *Phys. Rev. Lett.* **76**, 4689 (1996).
- [17] C. Kurtseifer, R.J.C. Spreeuw, M. Dresden, M. Wilkens, and J. Mlynek, "Classical and Nonclassical Atom Optics" in *Atom Interferometry*, ed. P.R. Berman, Academic Press, San Diego (1997), pp. 173-189.
- [18] W.R. Anderson, C.C. Bradley, J.J. McClelland, and R.J. Celotta, *Phys. Rev. A* **59**, 2476 (1999).
- [19] J.J. McClelland, *J. Opt. Soc. Am. B* **12**, 1761 (1995).
- [20] M.-O. Mewes, M.R. Andrews, D.M. Kurn, D.S. Durfee, C.G. Townsend, and W. Ketterle, *Physical Review Letters* **78**, 582 (1997).
- [21] V.I. Balykin and V.S. Letokhov, *Opt. Comm.* **64**, 151 (1987).
- [22] U. Janicke, M. Wilkens, *J. Phys. II France.* **4**, 1975 (1994).
- [23] B. Dubetsky and P.R. Berman, *Phys. Rev. A* **58**, 2413 (1998).
- [24] D.W. Keith, C.R. Ekstrom, Q.A. Turchette and D.E. Pritchard, *Phys. Rev. Lett.* **66**, 2693 (1991).
- [25] B. Dubetsky and P.R. Berman, in *Atom Interferometry*, edited by P.R. Berman, Academic Press, San Diego (1997), Chapter 10.
- [26] for example, see the review by K. Patorski, *Progress in Optics XXVII*, 1 (1989).
- [27] J.L. Cohen, B. Dubetsky, and P.R. Berman, <http://xxx.lanl.gov/abs/physics/9810043>.
- [28] B. Dubetsky, and P.R. Berman, *Phys. Rev. A* **59**, 2269 (1999).
- [29] A.G. Rojo, J.L. Cohen, and P.R. Berman (accepted for publication in *Phys. Rev. A*, Aug. 1999).
- [30] V.P. Chebotayev, B. Dubetsky, A.P. Kazantsev, V.P. Yakovlev, *J. Opt. Soc. Am. B* **2**, 1791 (1985).
- [31] H.F. Talbot, *Philos. Mag.* **9**, 401 (1836).
- [32] J.F. Clauser and M.W. Reinsch, *Appl. Phys. B* **54**, 380 (1992).
- [33] M.S. Chapman, C.R. Ekstrom, T.D. Hammond, J. Schmiedmayer, B.E. Tannian, S. Wehinger, D.E. Pritchard, *Phys. Rev. A* **51**, R14 (1995).
- [34] S. Nowak, Ch. Kurtsiefer, T. Pfau, and C. David, *Opt. Lett.* **22**, 1430 (1997).
- [35] J.P. Gordon and A. Ashkin, *Phys. Rev. A* **21**, 1606 (1980).
- [36] C.V. Raman and N.S.N. Nath, *Proc. Indian Acad. Sci.* **2**, 406 (1935)
- [37] C. Henkel, J.-Y. Courtois, and A. Aspect, *J. Phys. II (France)* **4**, 1955 (1994).
- [38] S.E. Koonin, *Computational Physics: FORTRAN version* (Addison-Wesley, Reading, MA, 1990).
- [39] Other definitions of the focal time are possible, such as the earliest time that maximizes the ratio or the difference between the peak and background densities, or the point where the peak-width product is a maximum. The definition we have chosen, the first maximum of $\rho(0, t)$, is sufficient to characterize the lens fully. Furthermore, this definition is consistent with the optical lens focus and leads to nearly identical results as a definition where the difference in central and background densities, $\rho(0, t) - \rho(\pi, t)$, is maximized. We also use the term *spot size* instead of line size or linewidth to refer to the HWHM of the focused line created by the one-dimensional SW lens.
- [40] I.S. Gradshteyn, I.M. Ryzhik, *Tables of Integrals, Series, and Products* (Academic Press, San Diego, CA, 1994).
- [41] The analysis of Ref. [28] can be generalized to an *open* system, where the excited state decays to many ground state sublevels including $|g\rangle$.
- [42] Note that by fixing $t_{0,f}$ we are not actually using the time $\bar{t}_{0,f}$ where the function $\bar{\rho}(0, t_0)$ is a maximum when evaluating $\bar{\rho}(0, t_{0,f})/\rho(0, t_{0,f})$. The correction is small even for the largest value of v plotted.
- [43] N. Lu and P.R. Berman, *Phys. Rev. A* **36**, 3845 (1987).
- [44] For this field area the Raman-Nath parameter (16) is relatively small, $\theta\omega_q\tau/3 = 0.21$.
- [45] see, for example, J. Schmiedmayer, M.S. Chapman, C.R. Ekstrom, T.D. Hammond, D.A. Kokorowski, A. Lenef, R.A. Rubinstein, E.T. Smith, and D.E. Pritchard in *Atom Interferometry*, ed. by P.R. Berman, Academic Press, San Diego (1997).
- [46] S.L. Rolston (private communication)